JOURNAL OF GEOPHYSICAL RESEARCH, VOL. 113, D12301, doi:10.1029/2007JD009277, 2008

Simulated lower stratospheric trends between 1970 and 2005: Identifying the role of climate and composition changes

Jean-François Lamarque,[1] D. E. Kinnison,[1] P. G. Hess,[1] and F. M. Vitt[1]

Received 13 August 2007; revised 24 December 2007; accepted 21 February 2008; published 18 June 2008.

[1] We have analyzed a set of simulations aimed at understanding the mechanisms that drive observed trends in the lower stratosphere after 1970. The simulations were performed using a version of the Community Atmosphere Model version 3 (CAM3) updated with interactive tropospheric and stratospheric chemistry. Even with a relatively low model top (≈40 km), this model shows good ability at reproducing a variety of large-scale changes in climate and chemical composition in the stratosphere when forced with the observed sea-surface temperatures and surface concentrations of long-lived trace gases and ozone-depleting substances. We then used the same model framework to differentiate the role of chemically active composition (ozone, methane, and chlorofluorocarbons) and CO_2 changes on observed trends in the stratosphere. Among the sensitivity factors analyzed, our simulations indicate that changes in CO_2 over the simulated period do not lead to significantly different total ozone trend; however, changes in CO_2 lead to important differences in ozone in the upper part of the model. On the other hand, changes in surface methane concentration are shown to play a significant role in driving changes in the globally averaged total ozone column, through a combination of changes in tropospheric and stratospheric ozone columns. We also show that the correlation between a change in tropical mean age of air and in vertical velocity breaks down above 20 hPa, in association with increased isentropic mixing above that level. Finally, we show that our model is capable of reproducing trends in the tropical age of air that were found in other studies; our simulations also indicate a significant impact of keeping methane and ozone-depleting substances at their 1970 levels, indicating the potentially important role of controlling methane emissions.

Citation: Lamarque, J.-F., D. E. Kinnison, P. G. Hess, and F. M. Vitt (2008), Simulated lower stratospheric trends between 1970 and 2005: Identifying the role of climate and composition changes, *J. Geophys. Res.*, *113*, D12301, doi:10.1029/2007JD009277.

1. Introduction

[2] The last decades of the 20th century have seen profound shifts in atmospheric composition [*Chipperfield and Fioletov*, 2007, and references therein], from the surface to the upper atmosphere. Among these changes, the decrease of ozone in the polar regions has been one of the most spectacular. It is now well established that the decrease of stratospheric ozone is due to heterogeneous chemistry on polar stratospheric clouds and requires the presence of chlorine- and/or bromine-containing compounds in sufficient quantities [*Newman and Rex*, 2007]. Most of those compounds, mainly the chlorofluorocarbons (CFCs) and their replacements, are man-made and have seen a dramatic increase in the release into the atmosphere, especially since the 1970s. The Montreal Protocol in 1989 has led to the regulation and subsequent decrease in emissions and concentrations of some of those compounds.

[3] At the same time, the atmosphere has also experienced a large increase in its concentration of long-lived greenhouse gases (CO_2, CH_4, and N_2O) which have contributed to the observed increase in surface and tropospheric temperatures. The roles of CH_4 and N_2O go beyond their radiative forcing and include a significant contribution to the chemistry of the troposphere and stratosphere [*Brasseur and Solomon*, 2005].

[4] The major goal of this paper is to investigate the role of CO_2 change (with its very strong impact on climate) and of chemically active composition change in observed trends in the stratosphere. As such, this paper complements the studies by *Dvortsov and Solomon* [2001], *Shindell and Grewe* [2002], *Austin and Wilson* [2006], *Butchart et al.* [2006], *Eyring et al.* [2006, and references therein], *Shindell et al.* [2006], *Austin et al.* [2007], *Garcia et al.* [2007], and *Olsen et al.* [2007]. In particular, the base simulations performed in this study are almost identical to those performed with the Whole Atmosphere Community Climate Model (WACCM) by *Garcia et al.* [2007], except for the vertical extension of the model (from the surface up to ≈40 km instead of ≈150 km in the case of WACCM) and a slightly different tropospheric chemistry scheme. As a

[1]Atmospheric Chemistry Division, Earth-Sun System Laboratory, National Center for Atmospheric Research, Boulder, Colorado, USA.

0148-0227/08/2007JD009277$09.00

result, our study also aims at estimating the ability of our model to reproduce observed trends as compared to the much more extensive representation of the stratospheric circulation in WACCM.

[5] One advantage of using a model simpler than WACCM is a significant (more than a factor of 2) reduction in its computational cost. This speedup allowed us to perform sensitivity studies in addition to the base case studies equivalent to *Garcia et al.* [2007]. In particular, we have performed an array of simulations (see Table 1) to discriminate between the effects of CO_2 changes and of chemically active constituent changes (such as methane and ozone-depleting substances).

[6] The paper is organized as follows: after the model description, we present in section 3 an evaluation of the mean atmospheric state, with an emphasis on its chemical composition. Section 4 discusses the ability of the model to reproduce many of the observed stratospheric trends. The specific role of CO_2 and composition changes is then analyzed in section 5 through a set of sensitivity simulations. Discussion and conclusions follow in section 6.

2. Model Description

[7] To perform the simulations, we use the Community Atmosphere Model version 3 (CAM3) [*Collins et al.*, 2006] modified to include interactive (i.e., with feedback to the radiation calculation in the atmosphere) chemistry, including aerosols, as in the work of *Lamarque et al.* [2005]. In order to simulate the evolution of the atmospheric composition over the last 35 years, the chemical mechanism used in this study is formulated to provide an accurate representation of both tropospheric and stratospheric chemistry.

[8] As a modification to the version discussed by *Lamarque et al.* [2005], we have introduced a reduced representation of hydrocarbon chemistry, following the work of *Houweling et al.* [1998], while the representation of methane oxidation is the same as in Model for Ozone and Related Tracers (MOZART) [*Horowitz et al.*, 2003]. Because of a significant underestimation of the formation of peroxyacetyl nitrate (PAN) using the Houweling et al. chemical scheme, we modified it to include PAN formation from reaction of OH with aldehydes (see their equation (R37)). This leads to a very reasonable simulation of PAN and other important chemical species as compared to aircraft observations (see auxiliary material[1]). In order to simulate the formation of secondary organic aerosols (SOA) from monoterpenes, we also included several additional chemical equations describing the oxidation path of monoterpenes, as done in MOZART [*Lack et al.*, 2004]; other hydrocarbons leading to SOA formation were already included in the Houweling et al. chemical mechanism but aromatics are not yet included.

[9] As we aim to simulate stratospheric chemistry, we have eliminated the relaxation in the stratosphere to a climatology of ozone and other species (namely NO_x, N_2O_5, HNO_3, CH_4, and CO) that tropospheric chemistry models typically require; only the relaxation of N_2O (above 50 hPa) to climatological values is kept as its relaxation removal slightly decreased the stratospheric NO_x distribution. In order for the model to successfully simulate the chemistry above 100 hPa, we have also included a representation of stratospheric chemistry (including polar ozone loss in polar stratospheric clouds) from version 3 of MOZART (MOZART-3) [*Kinnison et al.*, 2007]. Heterogeneous processes on sulfate aerosols and polar stratospheric clouds (liquid binary sulfate, supercooled ternary solutions, nitric acid tri-hydrate, and water-ice) are represented following *Considine et al.* [2000]. Chemical kinetics rates follow JPL-2002 [*Sander et al.*, 2003], as in the work of *Garcia et al.* [2007].

Table 1. List of Experiments

CO_2	CH_4	SSTs	CFCs	Number of Realizations
Time-varying	time-varying	time-varying	time-varying	2
1970	time-varying	1970	time-varying	1
1970	time-varying	climatology	time-varying	1
Time-varying	1970	time-varying	time-varying	1
Time-varying	time-varying	time-varying	1970	1

[10] At the lower boundary, the monthly varying zonal-averaged distribution of CO_2, CH_4, H_2 and all the halocarbons (CFC-11, CFC-12, CFC-113, HCFC-22, H-1211, H-1301, CCl_4, CH_3CCl_3, CH_3Cl, and CH_3Br) are specified following the data sets used by *Garcia et al.* [2007]. Monthly mean emissions of ozone precursors are based on the POET database (available at http://www.aero.jussieu.fr/projet/ACCENT/POET.php, combined with the optimized biomass burning emissions from *Pétron et al.* [2004] for carbon monoxide) and are kept constant for the whole simulated period. The monthly mean time-varying observed sea-surface temperatures and sea-ice distribution are prescribed from the Hadley Centre reconstruction [*Rayner et al.*, 2003].

[11] In addition, we consider time-varying uniform emissions of a tracer used for diagnosing the mean age of air. The mean age of air of any model grid cell is estimated by finding the time at which the concentration at that location (in time and space) had the same value at its stratospheric entry point (i.e., the tropical regions at 100 hPa) [*Hall and Plumb*, 1994; *Hall et al.*, 1999].

[12] Rigid-lid dynamical and no-flux chemical upper boundary conditions are specified. While this is clearly an oversimplification, it is consistent with our goal of estimating if one can design a "simple" model that can capture the main observed lower stratospheric trends. In addition no variation in the solar cycle is considered; this latter characteristic is based on the expectation that this will be a small effect over the simulated region (see below). The monthly surface area density of stratospheric aerosols is based on SAGE observations and is used for its chemical effect only [*Garcia et al.*, 2007]. The calculation of the photolysis rates takes into account the column ozone abundance above the model top, the latter using WACCM simulation results.

[13] The model configuration used for this study is a horizontal resolution of 2° (latitude) by 2.5° (longitude) and 26 levels, from the surface to ≈40 km (with eight levels above 100 hPa). With this upper lid, only a fraction of the

[1] Auxiliary materials are available in the HTML. doi:10.1029/2007JD009277.

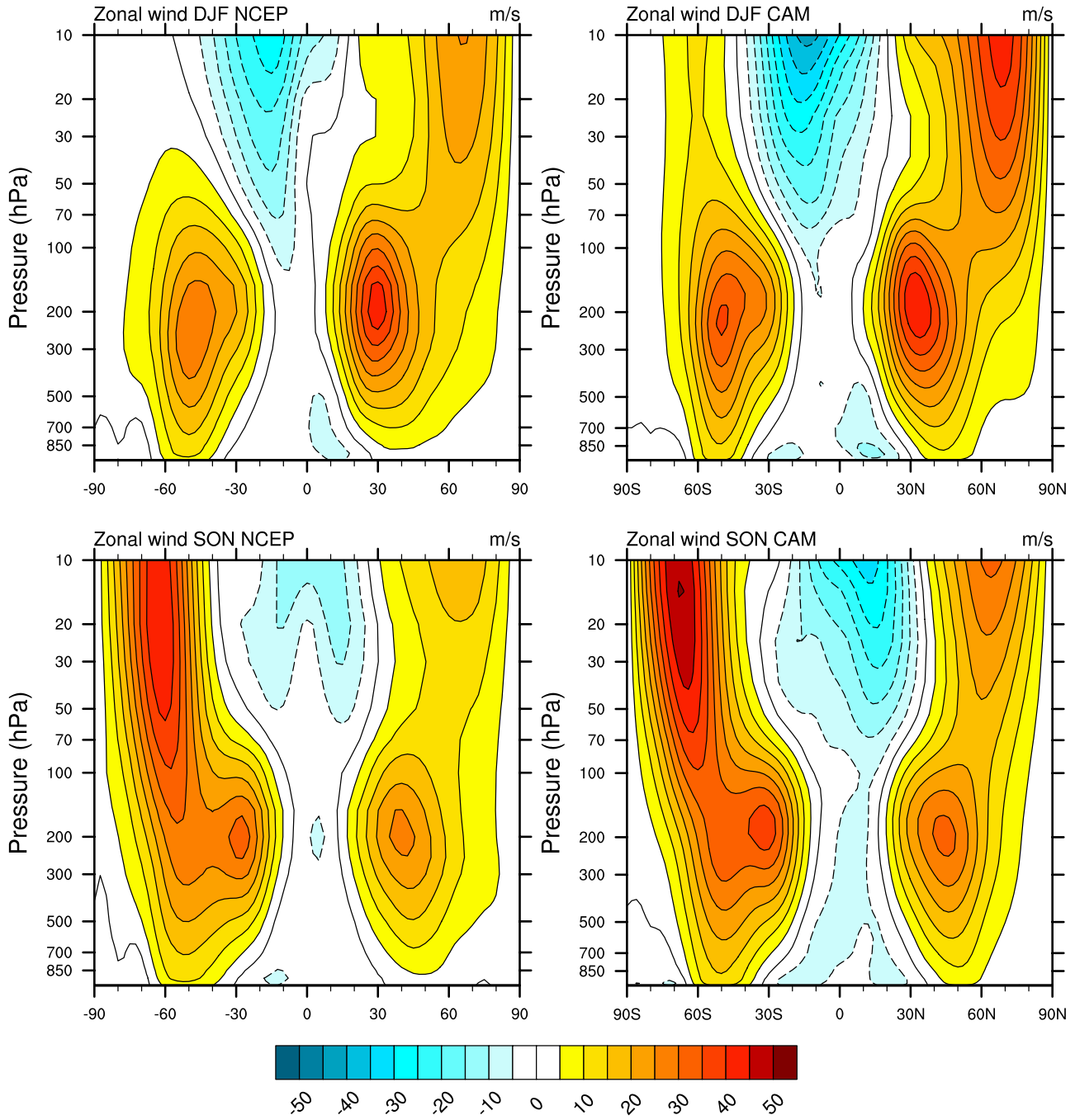

Figure 1a. Zonal average distribution of mean (1980–1999) zonal wind for (top) December/January/February and (bottom) September/October/November from (left) the NCAR/NCEP reanalyses and (right) the average of the two base simulations.

whole stratosphere is resolved; in particular, the region of maximum gravity-wave drag is located above the model top [*Garcia et al.*, 2007]. In order to still have a reasonable representation of the overall stratospheric circulation, the integrated momentum that would have been deposited above the model top is deposited in the top layer of the model.

[14] In many aspects, this model is set up exactly as for the experiments described by *Garcia et al.* [2007]. The only differences are a more extensive representation of tropospheric chemistry and, more significantly, the model vertical extent. Initial conditions (1 January 1970) for all chemical and meteorological fields are taken from the simulated 1970 distributions of *Garcia et al.* [2007]. Two realizations using this setup (simulations differing only by their initial conditions (chemical and dynamical), taken from two WACCM realizations of 1970, from *Garcia et al.* [2007]) were performed and cover the period 1970 through 2004. While changes in atmospheric composition started before 1970, many of the observational platforms were operational only

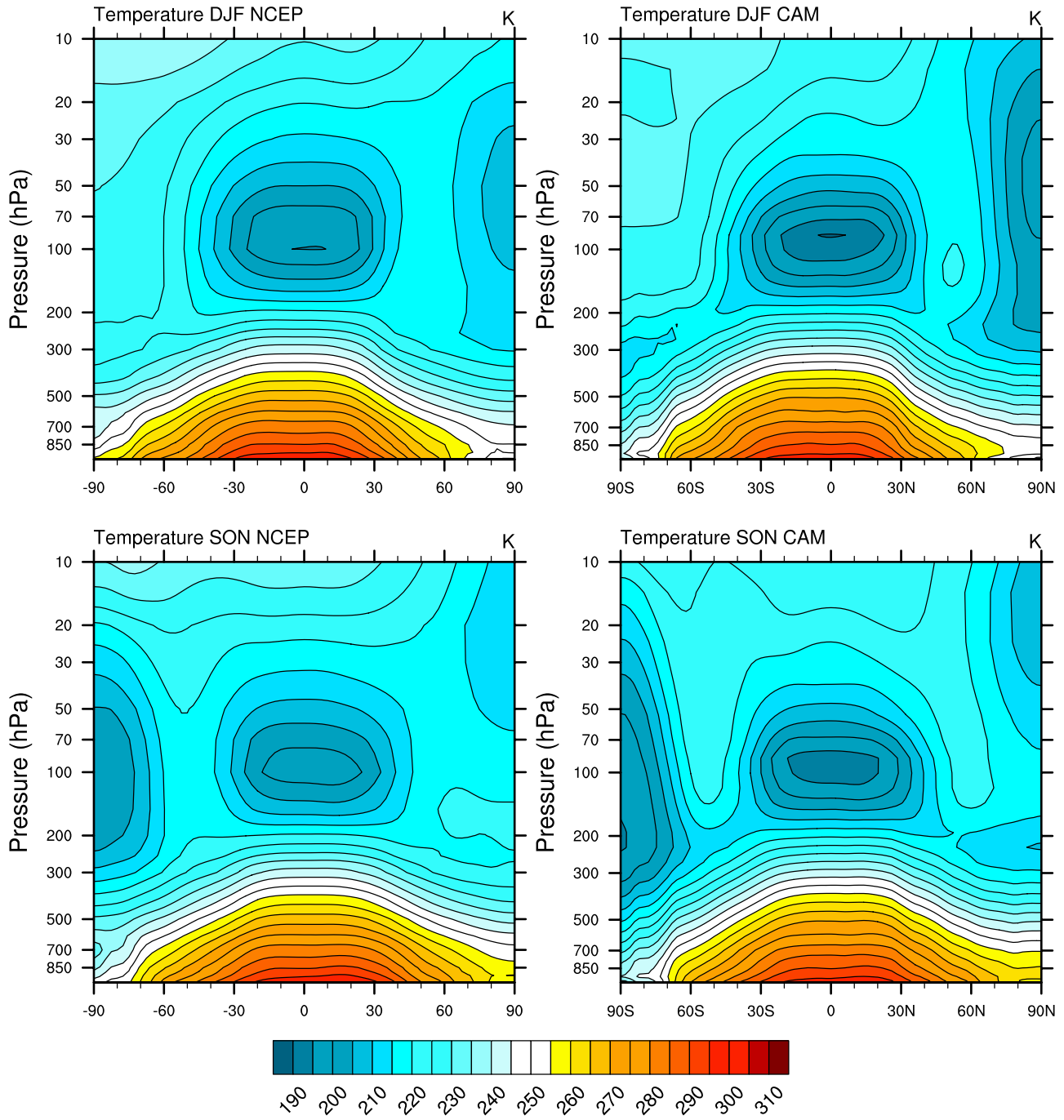

Figure 1b. Zonal average distribution of mean (1980–1999) temperature for (top) December/January/February and (bottom) September/October/November from (left) the NCAR/NCEP reanalyses and (right) the average of the two base simulations.

after 1980. This enables us to consider the first 10 years of each simulation as spin-up time.

3. Evaluation of Simulated Atmospheric Composition and Climate

[15] In this section, we discuss the main characteristics of the simulated mean climate and atmospheric composition. For this, we perform a comparison similar to the Chemistry-Climate Model Validation (CCMVal) analysis [*Eyring et al.*, 2006]. This comparison is made by averaging model results over the same period as the observational record, which in turns depends on the specific data set (see text and figure captions for more details).

3.1. Climatological Mean Zonal Wind and Temperature

[16] In order to gauge the accuracy of the simulated climatologies of zonal-mean zonal wind and temperature, we first compare them to the equivalent distributions from

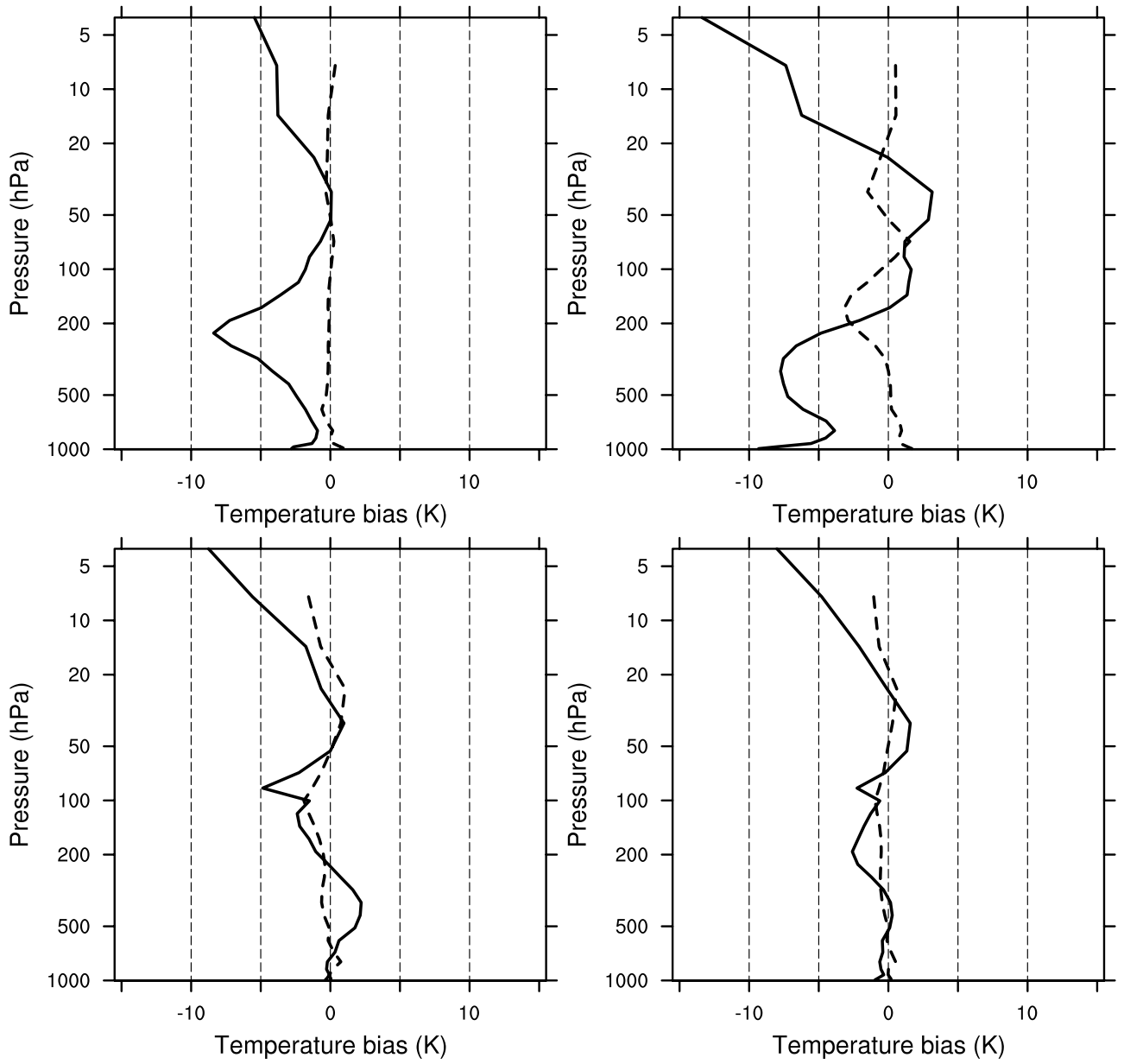

Figure 1c. Difference with respect to ERA-40 temperature for model simulations (solid) and for NCAR/NCEP (dashed). (top left) March/April/May 60°N–90°N; (top right) September/October/November 60°S–90°S; (bottom left) annual 30°S–30°N; (bottom right) annual 90°S–90°N.

the NCAR/NCEP (http://dss.ucar.edu/pub/reanalysis/) *Kalnay et al.* [1996] fields (Figures 1a and 1b, respectively). Because of the importance of winter and spring months on the chemistry of the stratosphere, we focus our analysis on December–February and September–November. We see that the overall structure of both fields (temperature and zonal wind) is well represented by the model. The main discrepancies are an overestimate of the polar zonal wind in winter, associated (through the thermal wind relationship) with the cold bias in the same region (Figure 1b). On the other hand, the position and strength of the midlatitude jets is in quite good agreement with the NCAR/NCEP distributions.

[17] For additional insight into the model biases, we compare the temperature distributions (Figure 1c) to the ERA-40 (ECMWF Reanalysis, http://www.ecmwf.int/research/era/) [*Uppala et al.*, 2005] reanalysis temperatures (1985–1999) for the Northern Hemisphere (60°N–90°N, March–May), Southern Hemisphere (60°S–90°S, September–November, as high-latitude temperatures in winter and spring are particularly important for correctly modeling PSC induced polar ozone depletion [*Eyring et al.*, 2006]), tropics (30°S–30°N, annual), and global (90°S–90°N, annual). As a measure of the representativeness of the ERA-40 temperatures, we also include the equivalent bias of the NCAR/NCEP (http://dss.ucar.edu/pub/reanalysis/) [*Kalnay et al.* [1996] reanalysis temperatures against ERA-40. The analysis is performed on the ERA-40 pressure levels.

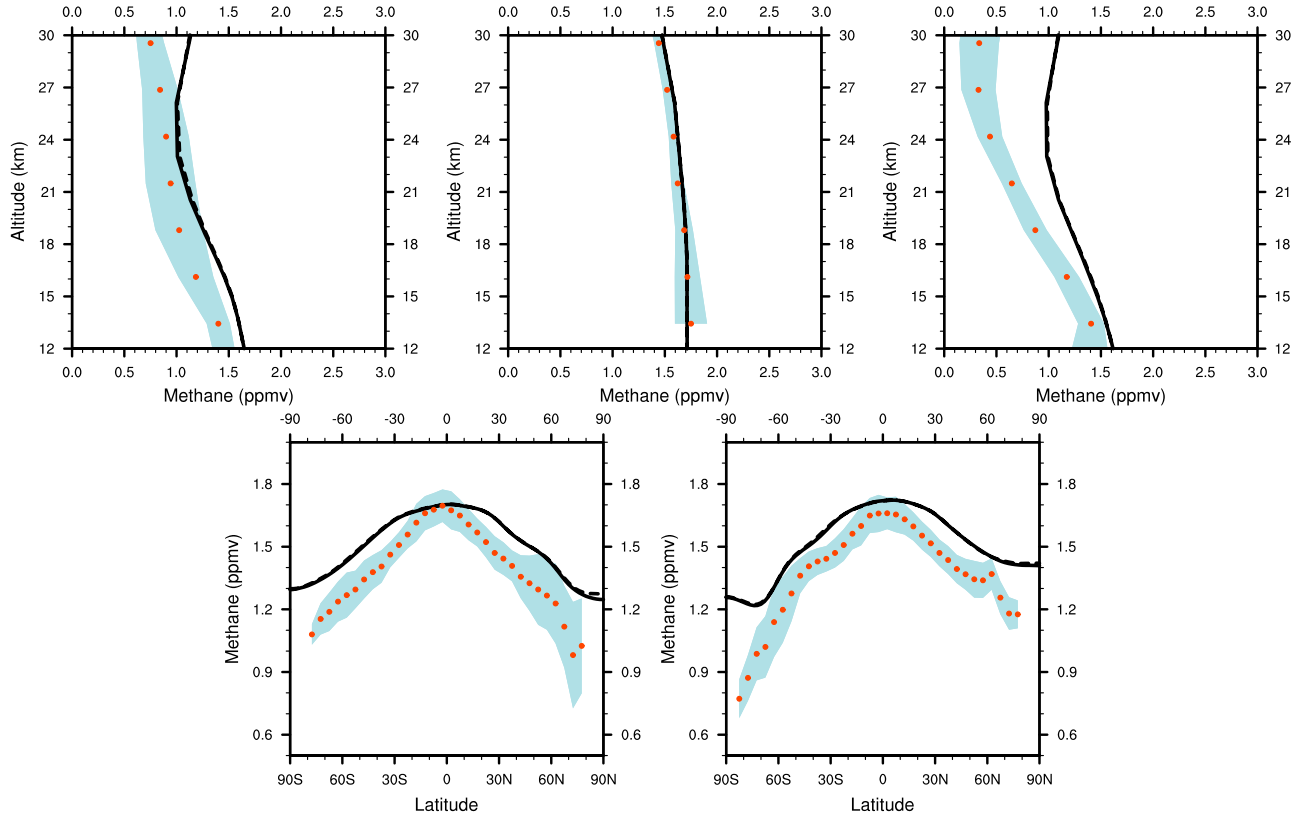

Figure 2. Comparison of the climatological methane distribution (for both simulations) with the HALOE climatology of *Grooß and Russell* [2005]. (top left) 80°N, March; (top middle) equator, March; (top right) 80°S, October; (bottom left) 50 hPa, March; (bottom right) 50 hPa, October. Observations are shown as red dots ±1 standard deviation about the climatological mean. Both model realizations are shown as solid and dashed lines.

[18] Over the polar regions, following the diagnostics of *Eyring et al.* [2006], we find that, in the upper portion of the model (above 20 hPa), the simulated temperatures are always biased low, by 5 to 10 K. In the region between 30 and 100 hPa, where most of the temperature-sensitive ozone depletion processes occur, the model is actually able to reproduce the climatological mean within a few degrees, very similar to the range of model results seen in the work of *Eyring et al.* [2006]. In the lower part of the model domain, the model is also biased low compared to the reanalyses. This is notably the case in the Northern Hemisphere around 200 hPa, a potential area for the formation of polar stratospheric clouds. Interestingly, in the troposphere, our temperature biases are very similar to the overall results of *Eyring et al.* [2006]; however, our stratospheric biases (above 20 hPa) tend to be larger, and of the opposite sign, to WACCM and other models in the work of *Eyring et al.* [2006]. There are also significant biases in the lower Southern Hemisphere troposphere, even though sea-surface temperatures are prescribed according to their observed values. This therefore points to problems in the representation of Southern Hemisphere climate and, in particular, the large biases in cloud cover in CAM3 [*Hack et al.*, 2006].

[19] In the tropical regions, where the ability to represent the cold-trap tropopause is key to the distribution of stratospheric water, the model tends to be slightly biased cold. This bias is consistent with the results of *Garcia et al.* [2007] and indicates that the stratospheric water vapor will be biased low (see section 3.2).

[20] In the global mean, except in the upper layer of the model, the climatological temperature is quite well reproduced; this could be expected as the model is strongly constrained at its lower boundary by the observed sea-surface temperatures and chemical composition.

3.2. Climatological Chemical Composition

[21] We compare here the simulated mean chemical constituents distribution to observed climatologies by the HALOE instrument on board the UARS satellite [*Grooß and Russell*, 2005], namely CH_4, H_2O, and HCl. As the focus of our analysis is on the stratosphere, we will only consider measurements above 12 km.

[22] Since methane is specified as a lower boundary condition based on observed surface concentrations, its distribution (Figure 2) in the tropical lower stratosphere is accurately represented. Because of the limited vertical extent of the model, mixing ratios in the polar regions are overestimated (especially in the Southern Hemisphere) due to the lack of photochemical loss in the middle to upper stratosphere (i.e., above the model top). This point is well illustrated by the zonally averaged figures.

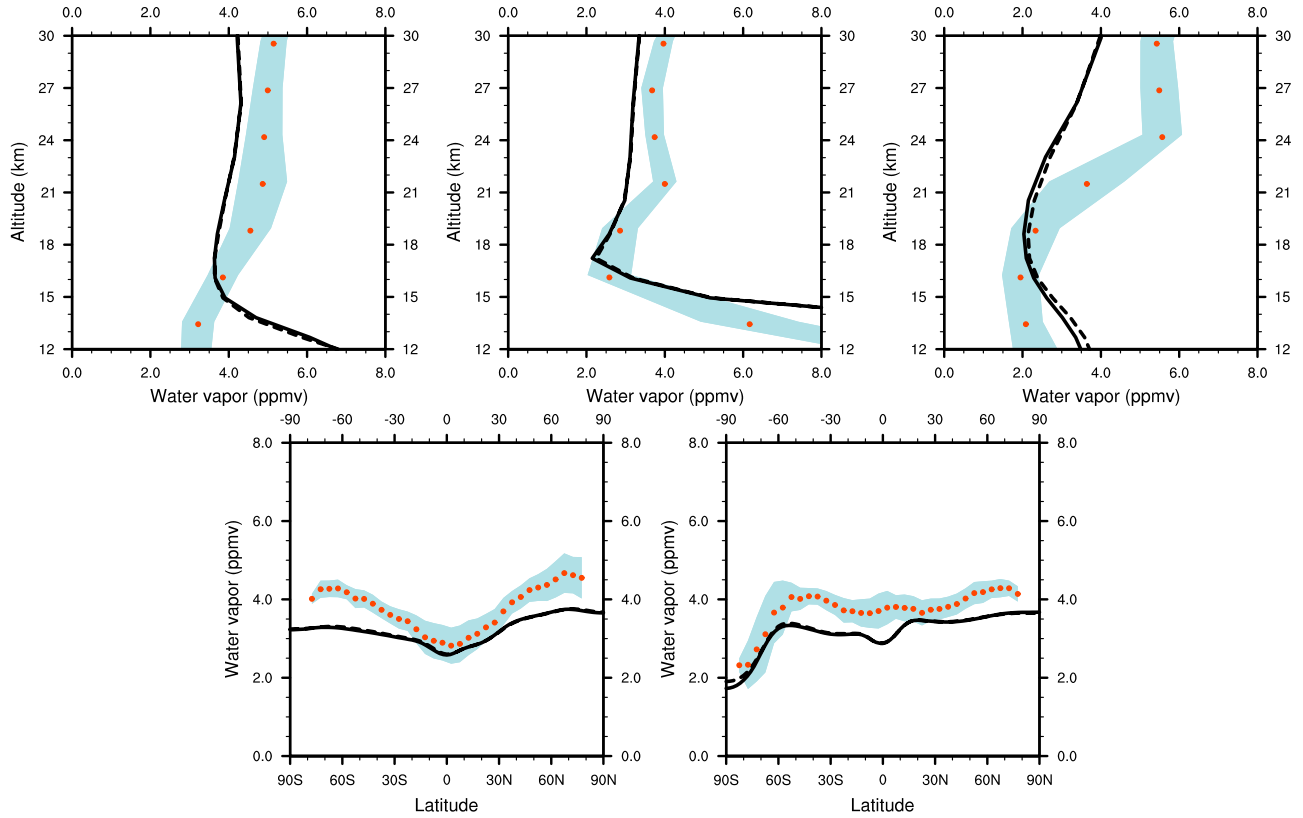

Figure 3. Comparison of the climatological water vapor distribution (for both simulations) with the HALOE climatology of *Grooß and Russell* [2005]. (top left) 80°N, March; (top middle) equator, March; (top right) 80°S, October; (bottom left) 50 hPa, March; (bottom right) 50 hPa, October. Observations are shown as red dots ±1 standard deviation about the climatological mean. Both model realizations are shown as solid and dashed lines.

[23] On the other hand, water vapor (Figure 3) tends to be biased low, as indicated in the previous section, in relation with a cold bias in the tropical tropopause temperature; this is accentuated in the upper stratosphere, where additional contribution from methane oxidation is also underestimated (see above). In the Southern Hemisphere polar region, it is worth mentioning that there is good indication that dehydration is realistically simulated by the model, albeit starting from lower mixing ratios than observed.

[24] An important measure of the potential for ozone loss is the stratospheric HCl concentration. It is also an indication of the integrated amount of CFC-photolysis that has occurred in the stratosphere (this is ultimately strongly related to the notion of age of air, see below). The HCl distribution (Figure 4) shows good agreement with the HALOE measurements throughout the stratosphere, and is very similar to that calculated by the collection of chemistry-climate models in the work of *Eyring et al.* [2006, Figure 12], except in the regions poleward of 80° in the spring which show some underestimate of the HCl concentration in the polar vortex. This underestimate is most likely associated with the model lid being at 4 hPa, limiting the ability of the model to create old air masses in the vortex, for which the photolysis of CFCs has had more chance to occur. On the other hand, the fact that the model has a reasonable representation of HCl is probably due to the fact that the model overestimates methane close to its upper lid, enabling a more rapid production of HCl from Cl reacting with methane [*Brasseur and Solomon*, 2005].

3.3. Climatological Mean Age of Air

[25] The ability of CAM3 to represent the mean age of air in the lower stratosphere (20 km) has been discussed by *Rasch et al.* [2006]. At that altitude, there is remarkable agreement between the SF_6 derived estimates [*Hall et al.*, 1999] and the model calculation (see their Figure 8). On the other hand, as can be expected from a model with a lid at 40 km, the ability to represent the mean age of air in the upper part of the model is quite limited (Figure 5). Our model is however capable of providing a distribution of the mean age of air that includes relatively old air (older than 4 years) in the polar regions, especially in the Southern Hemisphere (Figure 5); note that the two model realizations in Figure 5 show differences of up to half a year. The overall mean age of air distribution is actually quite similar to the results of *Austin and Li* [2006]. Therefore, even in our model with a fairly low model top, many of the mean age of air features found in the observations and in other models are found in our simulations. This is due to the fact that the residual circulation in the upper portion of the model is

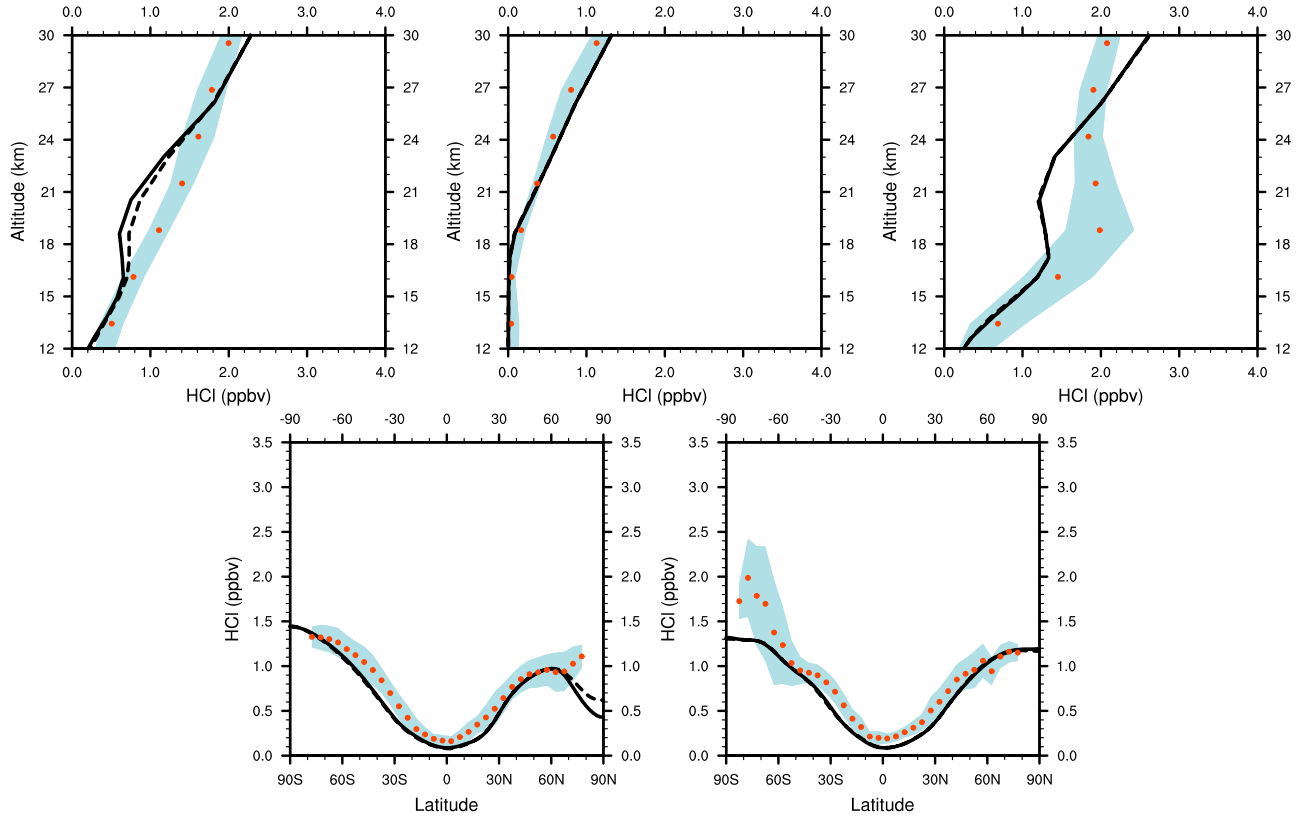

Figure 4. Comparison of the climatological HCl distribution (for both simulations) with the HALOE climatology of *Grooß and Russell* [2005]. (top left) 80°N, March; (top middle) equator, March; (top right) 80°S, October; (bottom left) 50 hPa, March; (bottom right) 50 hPa, October. Observations are shown as red dots ±1 standard deviation about the climatological mean. Both model realizations are shown as solid and dashed lines.

actually slightly slower than in models such as WACCM (not shown).

4. Trends in Atmospheric Composition and Temperature

[26] The previous chapter provided an evaluation of the ability of the model to represent the observed climatology of temperature and chemical composition, with an overall reasonable climatology of wind and temperature, but with a negative bias in the northern polar regions and positive in the southern polar regions. On the composition side, the distribution of methane shows a positive bias in the upper part of the model, while HCl is very close to the observations. As a summary, one can say that the simulations are weakest at the model top, with influences into the winter polar regions (due to the overall stratospheric circulation) and quite good otherwise. Following this previous analysis, we can now focus on the changes over the simulated period. As in section 3, we will focus on temperature, chemical composition and age of air.

4.1. Temperature

[27] We follow in our diagnostics of temperature trends the discussions of *Eyring et al.* [2006] and *Garcia et al.* [2007]. For that purpose, we first present the vertical distribution of the temperature linear trend for 1979–1998, averaged between 70°S and 70°N (Figure 6). We can see that the model is quite able to reproduce the observed (from radiosondes and satellite data) linear trend; our results are remarkably similar to *Garcia et al.* [2007], even in the details such as the larger (more negative) than observed trend between 5 and 10 hPa.

[28] Compared to the ERA-40 and NCEP 50 hPa reanalyses (Figure 7), the model is quite able (see list of linear trend estimates in Figure 7; note that the linear trend is calculated for all records using only the 1980–2001 period for consistency with the limited ERA-40 record) to represent the long-term linear trend of the temperature anomaly (temperature anomalies are calculated as deviations from a mean reference period between 1980 and 1989 using 3-month averages, as in the work of *Eyring et al.* [2006]). It is however clear that the lack of temperature impact from volcanoes (mainly El Chichon in 1982 and Pinatubo in 1991) hinders the model's ability to represent some of the observed interannual changes in stratospheric temperature. In the Northern Hemisphere, the model estimated linear trend agrees quite well with the analyses (note that the error estimate on the linear trend is on the order of 0.3–0.5 K/decade). In the Southern Hemisphere it is interesting to note that the two reanalyses show different behaviors, especially in the Southern Hemisphere in 1999–2001. This stands out because ERA-40 does not extend past August 2002. It is also interesting to note that, for that region, our

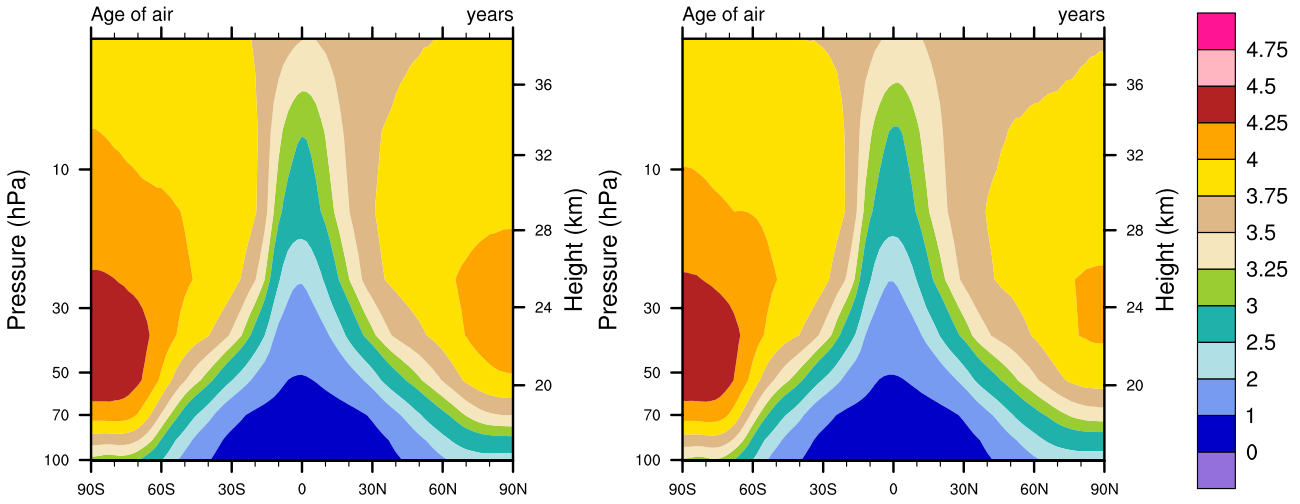

Figure 5. Zonal-mean distribution of the simulated stratospheric age of air (1995–2004 average) in years for the two base simulations (see Table 1). Estimates from observations [*Waugh and Hall*, 2002] at 20 km are on the order of 1–2 years in the tropics, 2.5 years at 30°N, and 5 years poleward of 60°N.

two realizations exhibit divergent trends in the early part of the 21st century. Interestingly, the error estimate on the linear trend calculations for the Southern Hemisphere is also on the order of 0.3–0.4 K/decade. At the global scale, there is better agreement between the simulations and the reanalyses (the error estimate is in all cases less than 0.15 K/decade), with however not quite enough cooling in the later part of the analysis record (beyond 1995). This is indeed a combination of the positive and negative biases found in the Northern and Southern Hemispheres, respectively. Similar conclusions can be drawn for the 70 hPa temperatures (not shown).

[29] As a partial conclusion, one can say that while the linear trends are quite well represented by the model, it is also clear that the simulated and observed interannual changes (and therefore the correlation on those timescales) are somewhat different, especially for the Southern Hemisphere. It is also clear that there is quite a difference between the ERA-40 and the NCEP temperature anomalies, especially for the late 1990s and early 2000s. Finally, it is important to note that the model performance is within the range of models analyzed by *Eyring et al.* [2006, Figure 4].

4.2. Chemical Composition

[30] The simulated stratospheric amount of inorganic (Cl_y) chlorine (Figure 8) has gradually increased until the early 1990s, mostly leveling off afterward. The model tends to underestimate the 1992 observations (by about 10%) and does seem to reach a more well-defined plateau after 1992 than observations suggest.

[31] Associated with this increase is the development of an ozone hole, mainly in the Southern Hemisphere but also in the Northern Hemisphere. Using the estimated net change in total ozone column from 1979 to 2005 [*Randel and Wu*, 2007], we see that the model (Figure 9) provides an overall realistic distribution and amplitude. One discrepancy is that the South Pole ozone hole tends to start later than in the observations (see the −70% line contour at 65°S in September), similar to *Garcia et al.* [2007]; the local minimum in the total ozone column change (between 60°S and 90°S) in February is however well-captured. There is also indication that the model slightly overestimates the North Pole ozone hole (mostly at its very minimum in March, poleward of 60°N, which is deeper than observations indicate), due to a cold bias in the lower stratosphere in that region, possibly in association with a too-small gravity wave drag (R. Garcia, personal communication, 2007). However, in the WACCM3 runs reported by *Garcia et al.* [2007], the NH polar stratosphere is a bit too warm, so they actually underestimate heterogeneous ozone loss. Another possibility for the cold bias is the representation of dynamical processes along and across isentropes, as CAM3 with a vertical isentropic coordinate

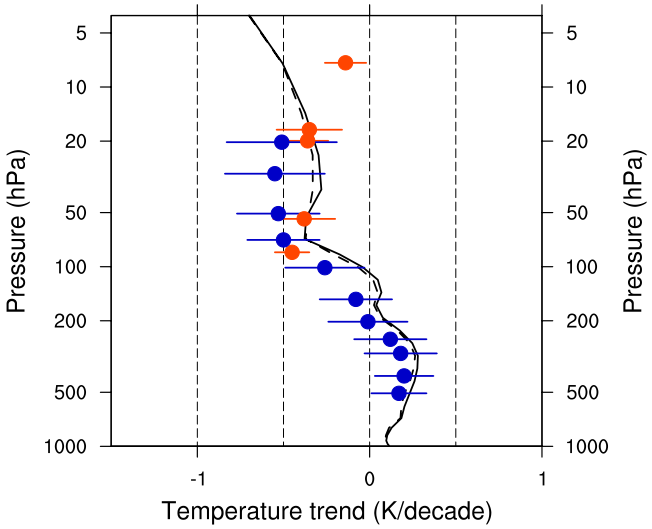

Figure 6. Linear temperature trend (70°S–70°N) between 1979 and 1998 from the model results (solid and dashed lines), radiosondes (blue circles), and satellite (red circles). See *Garcia et al.* [2007] and *Baldwin and Dameris* [2007] for details.

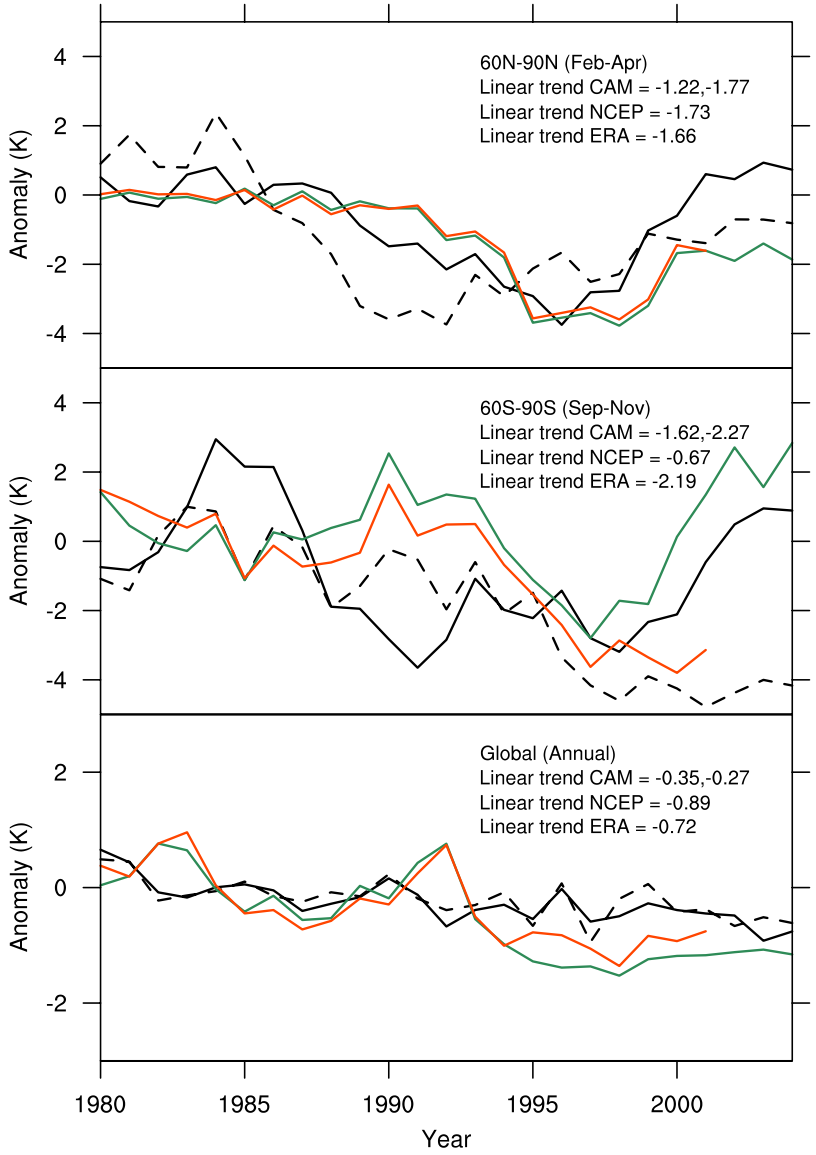

Figure 7. Temperature anomaly and linear trend estimate (K/decade) at 50 hPa from the model simulations (solid and dashed black lines), ERA-40 (red line), and NCAR/NCEP (green line).

configuration indicates a decrease in this bias (P. Rasch, personal communication, 2007). However, the trend in the northern midlatitudes (identified by the −12 and −16 DU contours) is quite well-captured; this is also true for the Southern Hemisphere.

[32] Averaged between 60°S and 60°N [*Chipperfield and Fioletov*, 2007], the model (Figure 10) reproduces the overall decrease in ozone from the early 1980s; as in the case of temperature, there is a clear signature from the large volcanoes that the model does not capture. A surface area density time-varying climatology (based on observations, see section 2) is used in the chemistry module for heterogeneous reactions but not in the photolysis. No volcanic aerosol effect is included in the calculation of radiative heating rates in the model. It also seems that the 60°S–60°N column anomaly from *Chipperfield and Fioletov* [2007] differs (is larger than) from the similar figure published by *Chipperfield and Randel* [2003], especially with respect to the deep minimum in 1985. Finally, note that the WACCM simulations in the work of *Garcia et al.* [2007] show a decrease after Pinatubo (1992–1993) on the order of 4%, larger than the 3% found in our simulations. Also, both models (WACCM and this model) indicate a recovery (from the 1992–1993 minimum) in the mid-1990s.

[33] With respect to the vertical distribution of the net ozone change for 1979–2005 (Figure 11), the model captures many of the observed changes [*Randel and Wu*, 2007], both in location and amplitude. While the absolute minimum in the southern polar regions (at 100 hPa) is underestimated by about 10%, tropical changes are well-represented. A preliminary analysis of the lower stratospheric tropical ozone trend in the model indicates that it could be mostly related to changes in the residual circulation (not shown). Overall, ozone changes in the northern polar regions are in reasonable agreement with the estimated values, with a significant trend (between −5 and −10%)

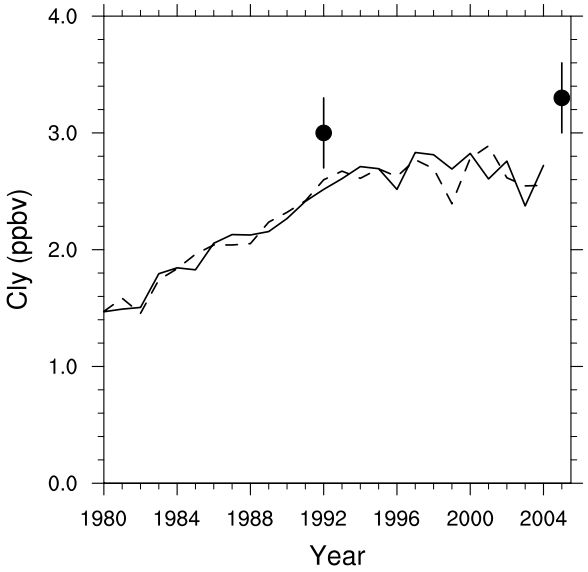

Figure 8. Time evolution of the November total inorganic chlorine at 50 hPa and 80°S from the model simulations (solid and dashed lines) and observations. See *Eyring et al.* [2006] for details.

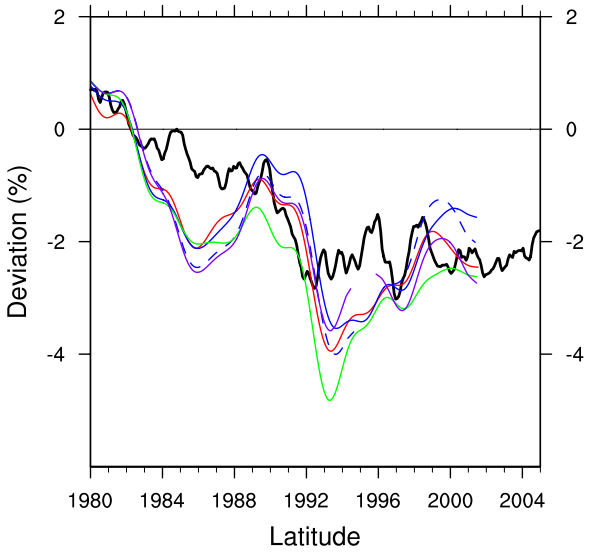

Figure 10. Deseasonalized area-weighted (60°S–60°N) total ozone deviation in the model (black line, deviation from 1970 to 1979 average, average of both simulations) compared to different global data sets (colored lines, deviation from 1964 to 1980 average). See *Chipperfield and Fioletov* [2007] for details.

between 300 and 70 hPa. As expected from Figure 9, the simulated trend in that region is slightly larger than observed. Finally, the slightly positive values in the tropical ozone trend of *Randel and Wu* [2007] are not found in our simulations; however, the latter is not statistically significant in the observational record.

[34] As seen in Figure 10 (and as can be expected from the changes in Cl_y shown in Figure 8), there is an indication of an "ozone recovery" after 1996. At this point, we have not analyzed if this "recovery" is related to a flattening of chlorine levels or still a recovery from Pinatubo. If one calculates the separate trends (1979–1995 and 1996–2005, as in the work of *Weatherhead and Andersen* [2006]), we see (Figure 12) that for both periods, the model tends to underestimate the measured ozone column trend. It does, however, capture the decrease and recovery and their latitudinal distributions; note that the measured trends in the observations are statistically significant mostly for the middle and high latitudes only [*Weatherhead and Andersen*, 2006] (note that this information is not displayed in Figure 12).

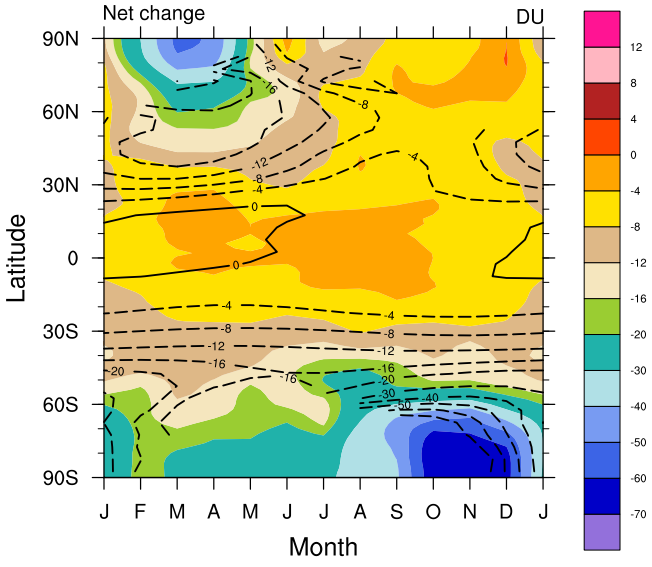

Figure 9. Net total ozone column change (1979–2005). Color contours are for the model results (average of both simulations) and line contours are from TOMS/SBUV [*Randel and Wu*, 2007].

[35] Trend estimates for water vapor are notoriously difficult to calculate, leading to differences between estimates from the satellite and radiosonde records [*Randel et al.*, 2004; *Austin et al.*, 2007], and are very sensitive to the analysis period [*Garcia et al.*, 2007]. Our estimate for the zonally averaged stratospheric water vapor trend is very similar to *Garcia et al.* [2007] (with a stratospheric increase on the order of 2–4%/decade above 20 km, and away from the polar dehydration regions, not shown), and therefore does not show very good agreement with the HALOE trend (which shows decreasing water amounts in the lower stratosphere with large increases above). It is interesting to note that our model (sampled as averaged over the 55°–70°N latitudinal band) seems to capture the interannual variability found in the POAM measurements (Figure 13, note the different scale on the left and right axes). However, on the basis of the aforementioned difficulty with the analysis of the variability in water vapor, it is possible that this agreement is mostly fortuitous, in addition to the fact that the model only simulates approximately half of the observed signal.

4.3. Mean Age of Air

[36] Model studies [*Rind et al.*, 2001; *Austin and Li*, 2006; *Austin et al.*, 2007; *Garcia et al.*, 2007] have

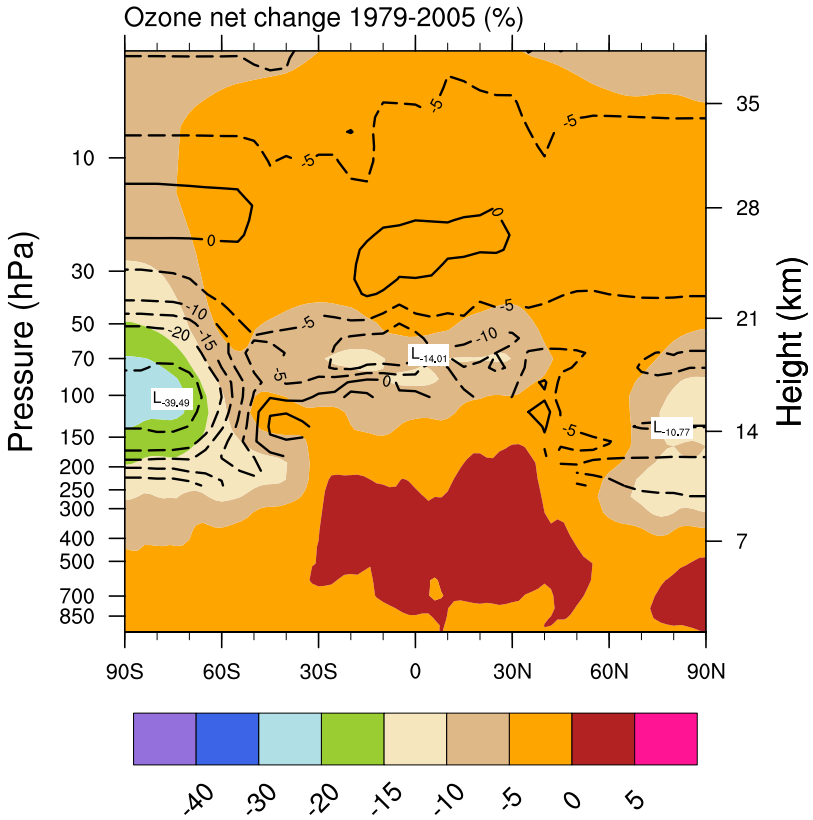

Figure 11. Vertical distribution of the zonal-mean annual-mean ozone net change (1979–2005). Color contours are for the model results (average of both simulations) and line contours are from TOMS/SBUV [*Randel and Wu*, 2007].

indicated the simulated mean age of air (specifically in the tropical regions and in the upper stratosphere) shows a decrease during the last few decades of the 20th century. Focusing on the 20°S–20°N region, our simulated mean age of air around 5 hPa shows (Figure 14) a clear decrease over the simulated period. Over 1980–2005, the model (in both realizations) exhibits a decrease of the mean age of air of approximately 0.15 year. This translates into a trend of 0.7 months/decade, slightly smaller than the estimated values of *Austin and Li* [2006] and *Garcia et al.* [2007] at ≈1.25 hPa; note however that in those studies, there is indication that this trend was faster prior to 1980.

[37] As noted in the work of *Garcia et al.* [2007], there is a good correlation in WACCM between the trend in the vertical velocity (which, in the tropics, is almost identical to the residual vertical velocity) and the trend in the mean age of air. This can be summarized by the following equation [*Garcia et al.*, 2007, equation (4)]

$$\delta\tau = -\frac{\tau^2}{\Delta Z}\delta w$$

where τ is the mean age of air, w the vertical velocity, ΔZ the altitude above the tropopause and δ indicates a perturbation from the long-term mean (for which $\tau = \Delta Z/w$). This relationship is the result of a simplification that arises because tropical vertical velocities in the lower stratosphere (especially above 70 hPa) are a weak function of Z in the WACCM or CAM runs, leading to the simple

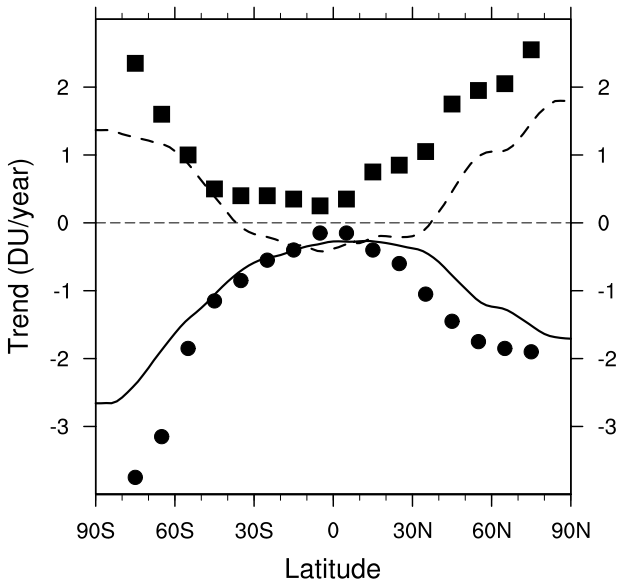

Figure 12. Measured and modeled total ozone column trends by latitude; 1979–1995 (black dots for the measurements and solid line for the model, average of both simulations) and 1996–2005 (black squares for the measurements and dashed line for the model). From *Weatherhead and Andersen* [2006].

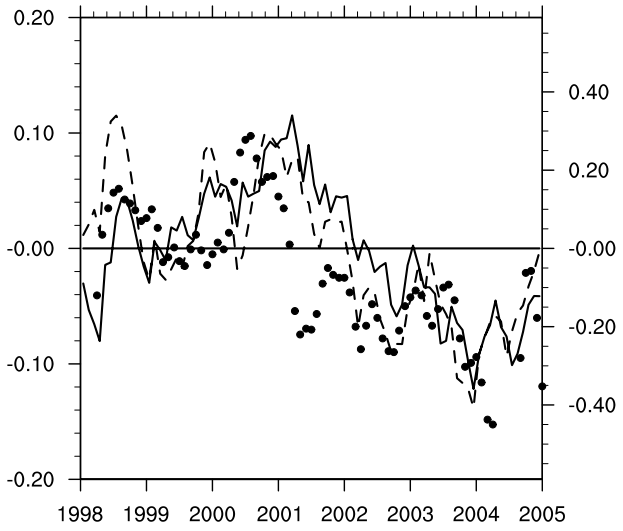

Figure 13. Time evolution (1998–2005) of the deseasonalized simulated water vapor deviation (ppmv) from the mean, averaged over 55°N–70°N at 85 (solid line) and 100 hPa (dashed line); the black dots are for the POAM-III measurements (right scale). See *Randel et al.* [2006] for details. Monthly data have been smoothed with a 1-2-1 running average. Note the different left and right scales.

inverse relationship between the mean age of air and the vertical velocity [*Garcia et al.*, 2007, equation (3)].

[38] To further analyze this relationship, we calculate the correlation between a perturbation (calculated here as the annual deviation from the long-term mean) in the vertical velocity at a specific level and the equivalent perturbation in the age of air (Figure 15a). The vertical distribution of this regression coefficient shows that the correlation is the strongest in the lower tropical stratosphere, reaching values close to 0 above 20 hPa (approximately a potential temperature of 700 K). Interestingly, this is the zone for which it has been estimated that isentropic mixing becomes large [*Minschwaner et al.*, 1996]; because of this increasing importance of mixing between tropics and extratropics, changes in mean age of air in that higher-altitude range are therefore only mildly related to changes in the stratospheric residual circulation. This also shows that the impact of vertical velocity changes on the mean age of air is either limited to the tropical lower stratosphere or the impact at higher levels is masked by mixing; further implications are discussed in section 5.2. In addition, note the negative values in the upper part of the model, indicating the breakdown of some of the underlying assumptions.

5. Sensitivity Studies

[39] In this section, we explore the role of various factors in constraining the simulated trends. In particular, we explore the isolated role of CO_2 and SSTs change, methane, and CFCs through a suite of independent simulations (see Table 1). While this analysis only pertains to the simulated period, it has direct implications for the expected ozone recovery during the 21st century. As in the previous sections, we focus our analysis on the stratosphere.

[40] As listed in Table 1, we have performed two different "no climate change" experiments: in the first case, we keep the monthly surface CO_2 and sea-surface temperatures at their 1970 levels (similar to the SL1960/SL2000 of *Austin et al.* [2007]), thereby locking the model into permanent 1970 meteorological conditions. This is clearly a simplification as "meteorology" should depend on things other than CO_2 and SST (e.g., ozone and aerosol amounts), although it is likely that CO_2 and SST are the most important contributors. The year 1970 is characterized by weak El Niño conditions (as indicated by the negative values of the ENSO index, see http://www.cdc.noaa.gov/people/klaus.wolter/MEI) and by a slightly negative phase of the Arctic oscillation (see http://www.cpc.noaa.gov/products/precip/CWlink/daily_ao_index/month_ao_index.shtml). In the second case, we use the 1970 CO_2 level as well but we constrain the sea-surface temperatures to be the 1949–2005 average. The juxtaposition of those cases therefore illustrates the dependence of the results to the overall sea-surface temperature distribution.

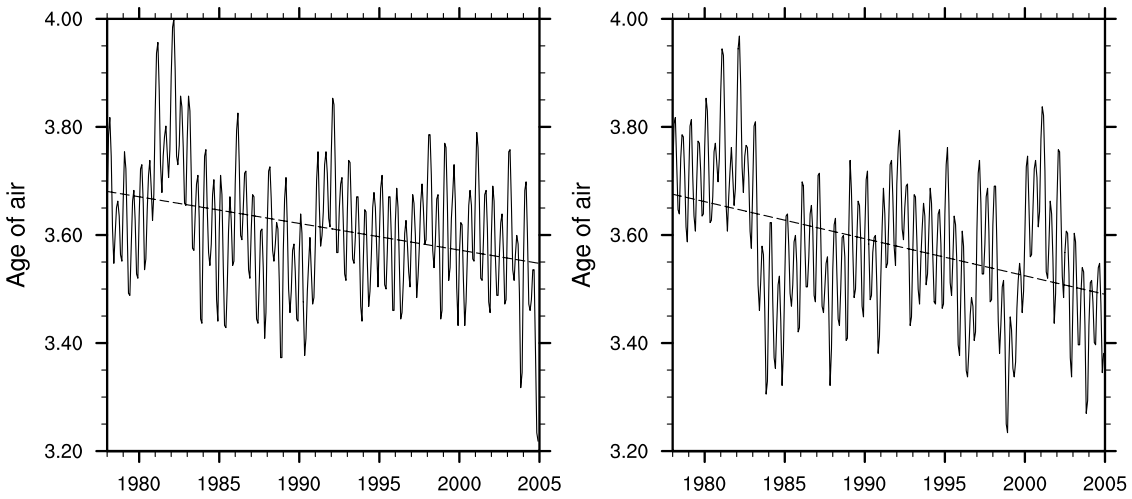

Figure 14. Time evolution of the monthly, zonally averaged, 20°S–20°N, age of air at 5hPa. The straight line is the least-square fit to the whole time series. Plots are for both realizations.

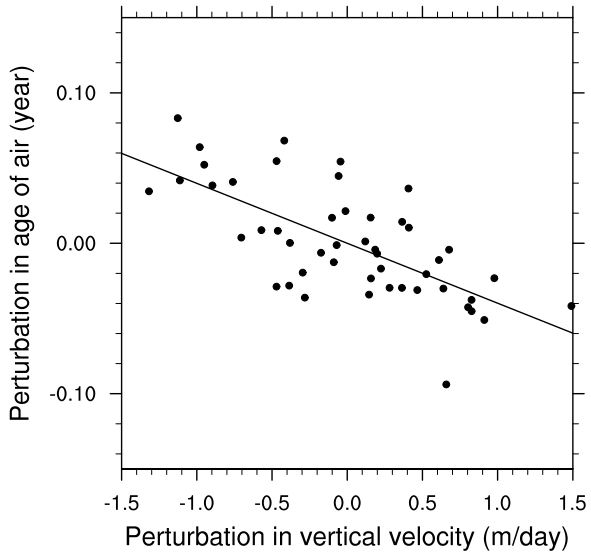

Figure 15a. Scatterplot of the perturbation (from the long-term mean, 50 hPa, 20°S–20°N) of the vertical velocity (horizontal axis) and the perturbation in age of air (vertical axis). Calculations are made for all years in both simulations. The straight line is the least-squares regression line through the cloud of points. See text and associated equation for details.

5.1. Total Ozone Column

[41] The sensitivity of stratospheric ozone to the climate state has been shown to be quite substantial in 21st century simulations [*Chipperfield and Feng*, 2003; *Chipperfield and Fioletov*, 2007, and references therein]. In our simulations, we look at this issue through the diagnostic of the globally averaged total ozone column change since the 1970s (Figure 16a). Regardless of the actual sea-surface distribution, we found that over the period 1970–2004, our simulated depletion of stratospheric ozone is not very sensitive to whether the effects of changes in CO_2 and SSTs are taken into account or not; this is, however, not the case in the upper part of the model (above 20 hPa, not shown), where ozone changes are found to be noticeably larger for fixed 1970 CO_2 levels (with either 1970 or climatological SSTs). The connection is through the inverse relationship between stratospheric temperatures and CO_2 levels [*Rind et al.*, 2001].

[42] Interestingly, our simulated response of the ozone total column to a fixed 1970 methane surface concentration (while CO_2 is allowed to change) is actually larger than the CO_2 effect (Figure 16a). By the end of 1990s, there is an increase of 2–3 DU (from −13 to −16 DU) in the (negative) ozone deviation with respect to the base simulations; using the two base case realizations as a rough estimate of significance, a difference of 2–3 DU might indeed be statistically significant. In the upper part of the model (above 50 hPa), we find that keeping CH_4 constant leads to less HCl (produced through the less-efficient reaction of Cl with CH_4 and therefore a smaller production of active chlorine in the PSC-processed air), with the overall consequence of a larger amount of ozone in the model than in the case of increasing methane. In terms of total ozone column change, the aforementioned effect of methane on stratospheric ozone is actually smaller than the effect of CO_2. This lower impact is however compensated in the integrated column by a smaller amount of ozone (about 2 DU around 2000) in the troposphere due to the lower levels of methane in that region (Figure 16b); a lower concentration of methane in the troposphere indeed directly translates into a decrease in tropospheric ozone [*West et al.*, 2006]. The combination of tropospheric and stratospheric responses leads to the overall large impact of methane on total ozone column, larger than the CO_2 effect.

5.2. Mean Age of Air

[43] Recent papers have discussed the link between changes in greenhouse gases and mean age of air [*Rind et al.*, 2001; *Austin and Li*, 2006; *Butchart et al.*, 2006; *Garcia et al.*, 2007]. We revisit this point by using the various sensitivity experiments. Our analysis has indicated a fairly significant mean age of air linear trend estimate sensitivity on the period over which the trend is calculated. Therefore, to alleviate some of that sensitivity, we look in this section at the difference between 10-year averages, namely 1980–1989 and 1995–2004; these estimates are not very different from linear trend estimates but were found to be more robust and so will be used here. For simplicity, in the rest of this discussion, we will describe this difference between 10-year averages (divided by the time difference between these averages) as trend. The zonal-mean distribution of the time evolution of the mean age of air (expressed as month/decade) shown in Figure 17 indicates that the base simulations (average of the two simulations, top left) yield to negative trends across the stratosphere. In particular, as discussed in section 4.3, the tropical average (whether 20°S–20°N, solid line or 30°S–30°N, dashed line), is on

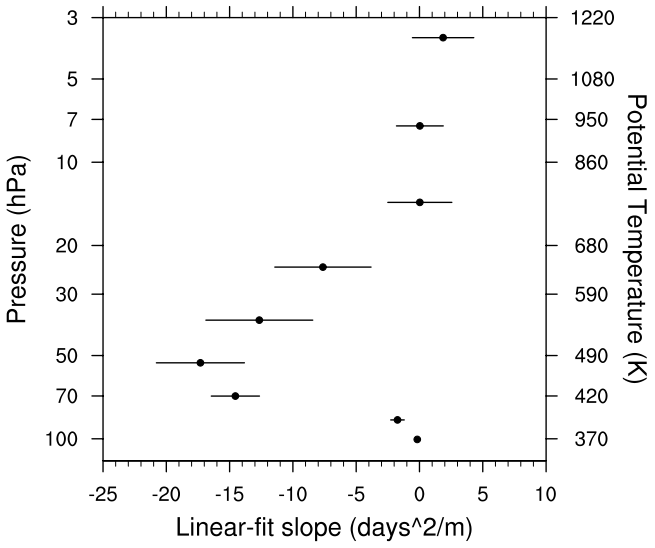

Figure 15b. Vertical distribution of the regression coefficient (horizontal bar is an estimate of the error on this coefficient) from Figure 15a. The potential temperature is shown on the right-hand vertical axis to compare with the estimates of isentropic mixing from *Minschwaner et al.* [1996]. See text and equation for details.

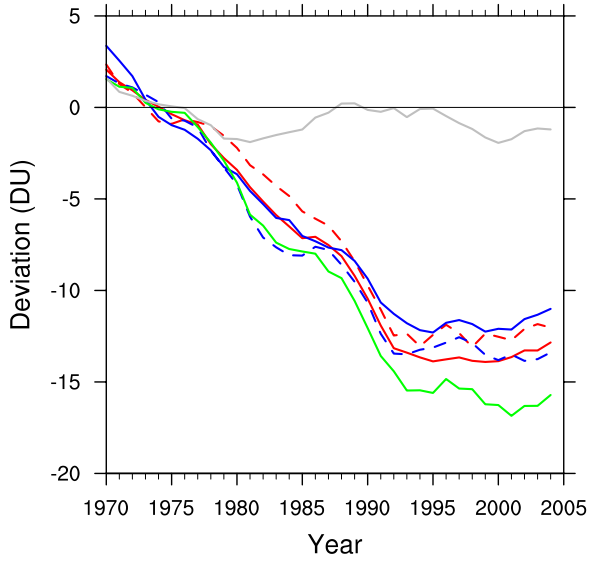

Figure 16a. Globally averaged total ozone column deviation (in Dobson Units) from the 1970–1979 average. Red lines are for the base simulations, blue lines are for the fixed 1970 CO_2 simulations (with 1970 and climatological SSTs, solid and dashed lines, respectively), green line is for fixed 1970 methane simulation, and silver is for the no CFCs simulation. Solid and dashed lines are for each realization of the same experiment. See Table 1 for details.

the order of 0.4–0.5 months/decade, reaching that value between 30 and 50 hPa.

[44] If methane surface concentration is held constant at its 1970 level, then a quite different mean age of air trend is simulated (top right), especially above 30 hPa. Indeed, what we find is a much reduced trend (close to 0 and even positive in some regions). Note, however, that for the tropical regions below 30 hPa, there does not seem to be much difference in the trend. In order to understand these stratospheric changes in the mean age of air, we first focus our analysis on changes (calculated again as the difference in 10-year averages) in zonal wind (Figure 18a); we focus our analysis here on the Northern Hemisphere and therefore limit our study to January–March (annual analysis leads to similar, albeit less clear signals). In the case of the base simulations (both simulations show very similar patterns), there is a very strong increase in the zonal wind across the simulated atmosphere (note that the bottom of the plot is here the surface). This is clearly linked with changes in the distribution of temperature (not shown) through the thermal wind relationship.

[45] As discussed in the work of *Rind et al.* [2001], the existence of a positive anomaly in the zonal wind distribution at the midlatitudes tropopause has the implication that waves (planetary and gravity) can more easily propagate upward. This increased propagation has then the effect of increasing momentum deposition where those waves break. In particular, momentum deposition associated with gravity waves (Figure 18b) shows a much larger amplitude (in absolute value) for the base simulations, indicating the presence of enhanced residual circulation [*Andrews et al.*, 1987] in those simulations; this forces the mean age of air to decrease by the overall acceleration of the residual circulation. It is this collection of features that enables the mean age of air trend to be quite different between the base simulations and the fixed 1970 methane simulation. It is, however, still unclear what the actual mechanism is, as we only illustrate here consistent patterns of differences. In addition, because most of gravity-wave momentum deposition is specified to occur at the model top, it remains to be seen if the same behavior will be observed if a model with a higher model top is used.

[46] As the direct radiative forcing of methane is overall fairly weak, this forcing cannot by itself change the temperature distribution in such a way that it would lead to an overall modification of the stratospheric circulation. On the other hand, this analysis (and the study by *Rind et al.* [2001]) suggests that a change in the position and strength of the tropospheric jet could lead to changes in the vertical propagation and ultimately breaking of waves in the stratosphere and the associated forcing of the residual circulation. Unfortunately, we do not have in the simulations discussed here the model output necessary to further analyze this hypothesis.

[47] When surface CO_2 and sea-surface temperatures are at their 1970 levels, the mean age of air in the upper part of our model shows an overall structure quite similar to the mean of the base cases but with slightly larger negative trends throughout the Northern Hemisphere stratosphere. This hemispheric difference was also noted by *Shindell et al.* [2006] and *Olsen et al.* [2007]. However, *Olsen et al.* [2007] indicates a significant response to the change in sea-surface temperatures alone. In addition, our response to CO_2

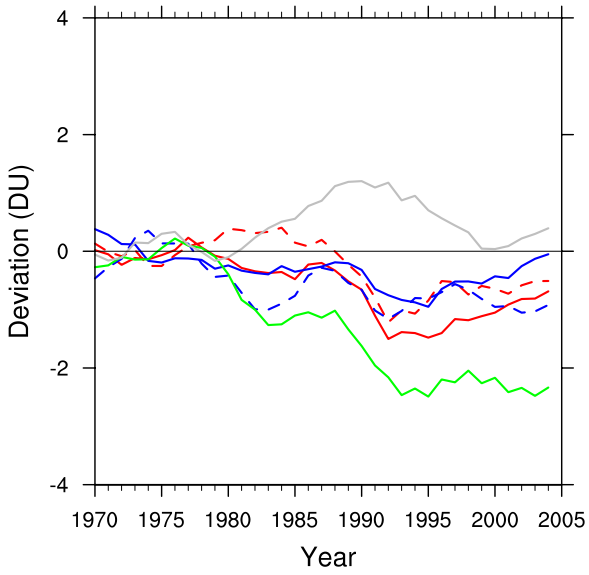

Figure 16b. Globally averaged ozone column below 200 hPa deviation (in Dobson Units) from the 1970–1979 average. Red lines are for the base simulations, blue lines are for the fixed 1970 CO_2 simulations (with 1970 and climatological SSTs, solid and dashed lines, respectively), green line is for fixed 1970 methane simulation, and silver is for the no CFCs simulation. Solid and dashed lines are for each realization of the same experiment. See Table 1 for details.

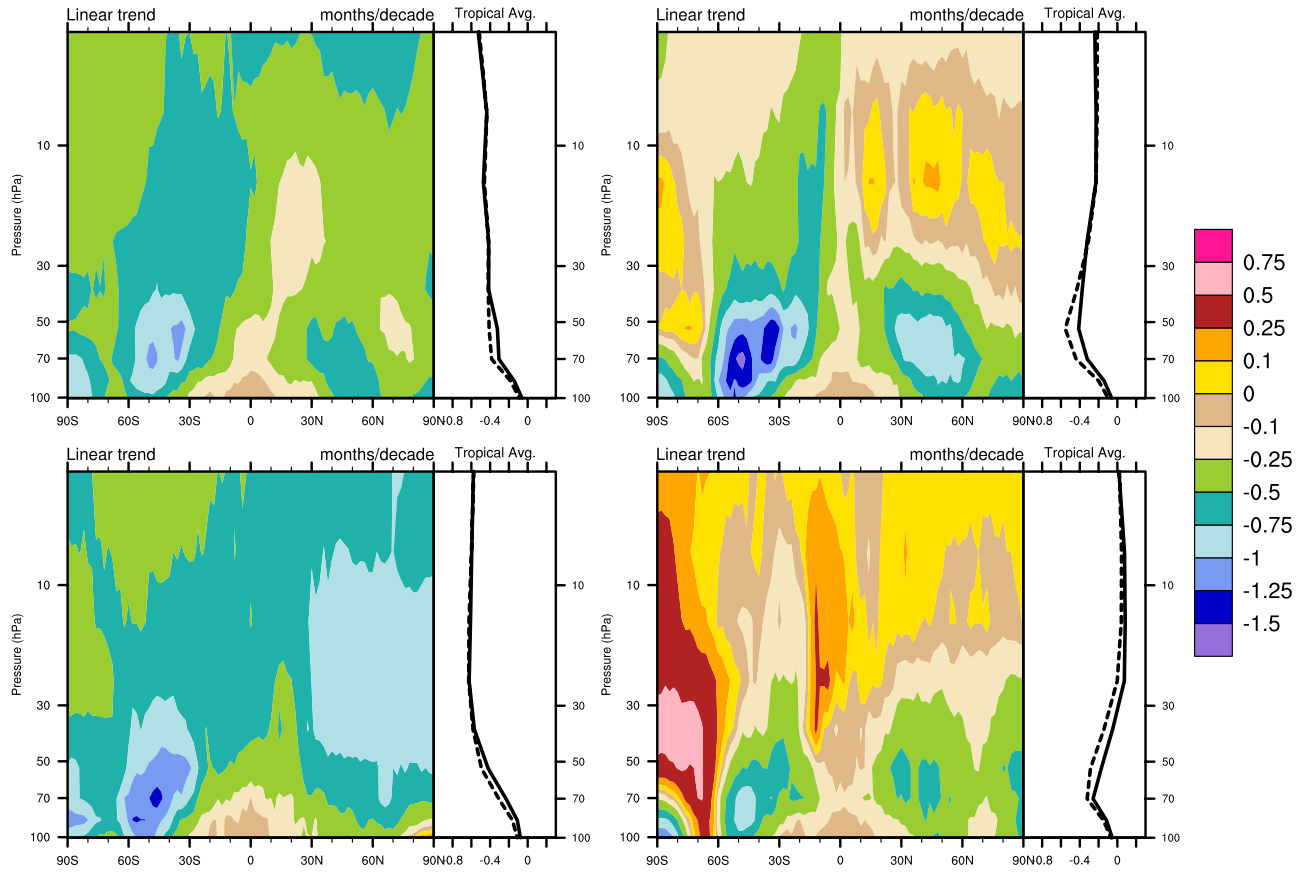

Figure 17. Zonal mean linear trend (in months/decade) of the stratospheric mean age of air. The line plots represent the vertical distribution of the average over 30°S–30°N (dashed line) and 20°S–20°N (solid line). (top left) Base case (average of two realizations), (top right) fixed 1970 methane case, (bottom left) fixed 1970 CO_2 and SSTs case, and (bottom right) fixed 1970 CFCs case.

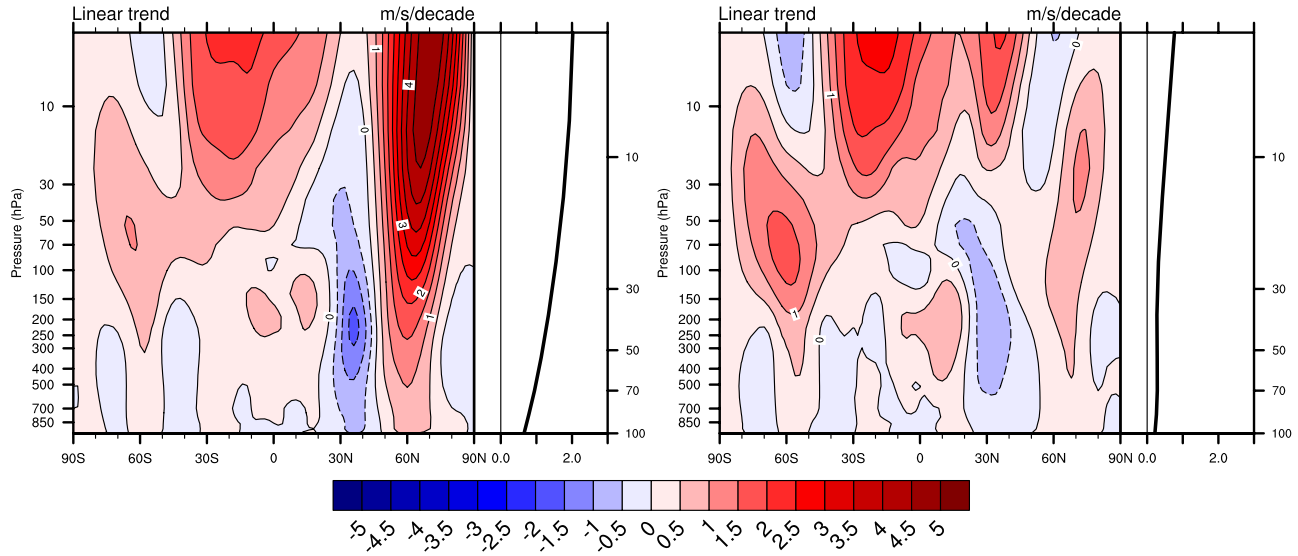

Figure 18a. Zonal mean linear trend (in m/s/decade) of the January–March zonal wind. The line plots represent the vertical distribution of the average over 30°N–90°N. (left) Base case (average of two realizations) and (right) fixed 1970 methane case.

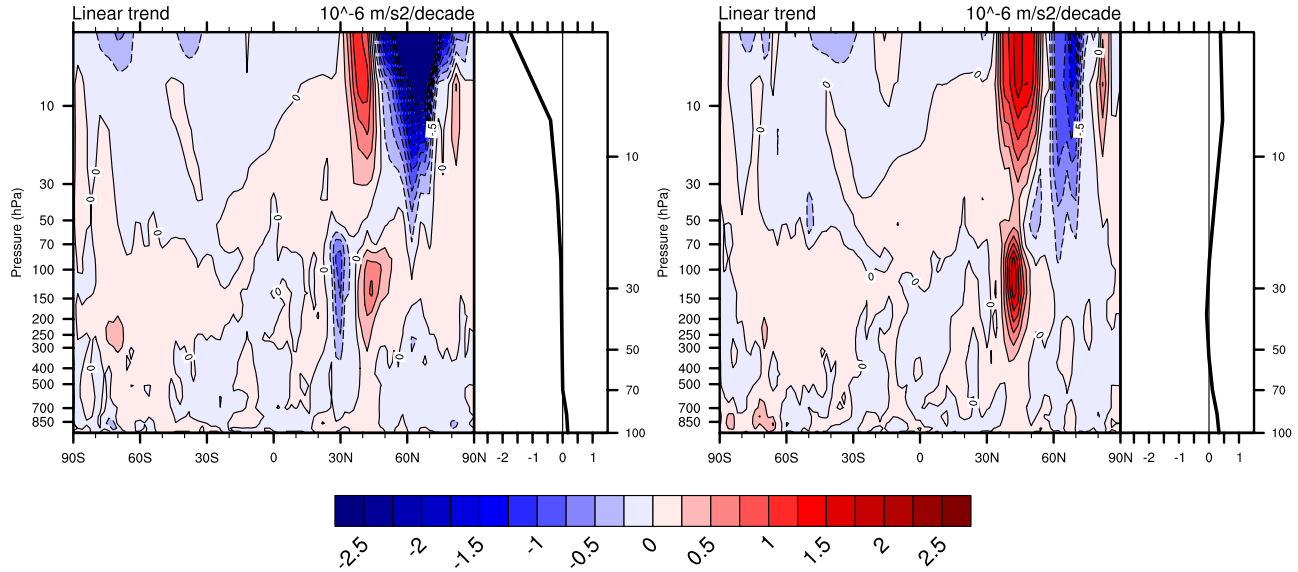

Figure 18b. Zonal mean linear trend (in 10^{-6} m/s^2/decade) of the January–March zonal wind tendency due to gravity wave breaking. The line plots represent the vertical distribution of the average over 30°N–90°N. (left) Base case (average of two realizations), and (right) fixed 1970 methane case.

and sea-surface temperatures is not as clear as the results of *Butchart et al.* [2006], possibly due to the smaller change in forcing and/or our shorter simulations. Finally, the case of constant 1970 CFCs indicate a response very similar to the fixed 1970 methane case, with little to no change in the mean age of air over most of stratosphere. In both cases, the changes in zonal wind and gravity wave tendencies are qualitatively the same as the one explained for the case of methane (not shown). The much reduced trend in the mean age of air in the fixed CFCs case above 30 hPa is associated with a time evolution of the mean age of air which exhibits a minimum in the mid 1990s (Figure 19). Figure 19 also illustrates the overall difficulty in extracting a linear trend out of the time series. It also points to the necessity of extending our analysis to longer simulations to make sure the simulated changes in the mean age of air trends are robust and not only transient features.

[48] Another interesting point is the existence of a local minimum in the trend in the mean age of air between 30°S and 60°S in the lower stratosphere in all simulations (Figure 17), albeit with various amplitudes; similar results were found in the work of *Rind et al.* [2001] and in the WACCM model (R. Garcia, personal communication, 2007) showing that this feature is most likely independent of mid- to upper-stratosphere dynamics, i.e., processes that are not explicitly resolved in our model configuration.

6. Discussion and Conclusions

[49] In this paper, we have discussed a set of model simulations that describe the evolution of the atmosphere subject to changes in surface concentrations of CO_2, methane and CFCs, and sea-surface temperatures.

[50] Using a variety of observed concentrations and calculated trends, we have shown that our model, even with

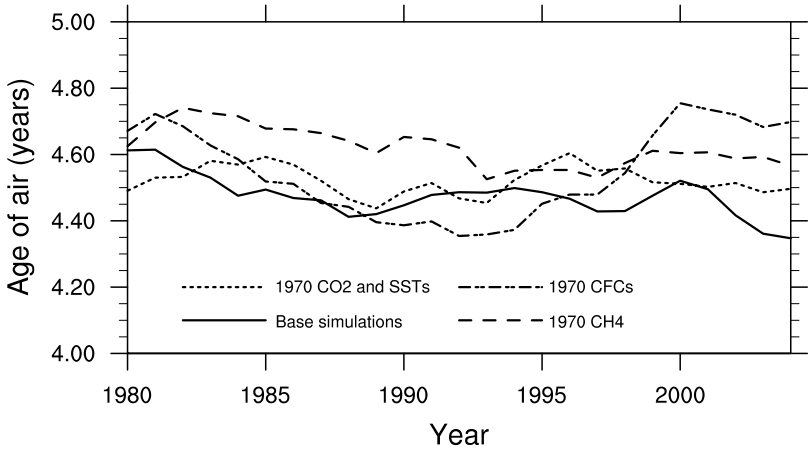

Figure 19. Time series of the annual-averaged mean age of air at 86°S and 50 hPa for a set of simulation (see legend). Each time series was smoothed using a 3-point (1-2-1) moving average.

the main limitation of having a relatively low upper boundary (around 40 km), was able to represent many of the observed stratospheric trends, in temperature and chemical composition, comparable in skill to many of the models in the work of *Eyring et al.* [2006]. Similarly we have shown that this model was able to reproduce the mean age of air trends that had been simulated using models with a more complete representation of the dynamical and chemical processes of the stratosphere and above [*Austin et al.*, 2007; *Garcia et al.*, 2007]. The model is however far from perfect, with a cold bias in the northern polar lower stratosphere, leading to an overestimate of the Arctic ozone hole.

[51] Our estimate of the simulated mean age of air is in agreement with the analysis of *Eyring et al.* [2006] and shows tendencies similar to the results of *Rind et al.* [2001], *Austin et al.* [2007] and *Garcia et al.* [2007]. Our simulated specific effect of CO_2 is smaller than other studies, but our limited simulation period might play a significant role in that limited signal; however, other studies did not distinguish between CO_2 and CH_4. We also show that the trend in the tropical age of air is strongly constrained by the trend in the vertical velocity up to 20 hPa (650 K); above that level, isentropic mixing between the tropics and the extratropics destroys the correlation found below that level.

[52] Over the analyzed period (1980–2005), changes associated with increasing CO_2 and sea-surface temperatures lead to very small changes in the globally averaged total ozone column. It is possible that these boundary condition changes were too small to produce the significant impact found in other (with longer considered time periods and associated CO_2 changes) studies [*Chipperfield and Feng*, 2003]. On the other hand, we found that keeping methane at its 1970 level has a significant impact on the evolution of the total ozone column. This impact is a combination of stratospheric (through changes in the ozone production rates) and tropospheric (through a decrease in the tropospheric amount of ozone). In our simulations, forcing surface concentrations of methane and CFCs to stay at their 1970 level has a significant impact on the trend of the mean age of air in the stratosphere above 30 hPa, more so than the effect keeping CO_2 and SSTs at their 1970 levels. This illustrates that controls of methane emissions can have potentially important roles, ranging from tropospheric ozone [*West et al.*, 2006] to stratospheric circulation, age of air, and stratospheric ozone recovery in the 21st century. Nevertheless, our analysis also illustrates the difficulty in comparing linear trends calculated over 25-year periods and clearly shows that additional simulations over longer periods will be necessary to fully assess the specific role of composition and climate on observed trends in the stratosphere.

[53] **Acknowledgments.** We would like to thank J. Orlando for his help in improving the representation of tropospheric chemistry in the model used in this study. J. Orlando and R. Garcia provided comments that greatly improved an earlier version of this manuscript. Three anonymous reviewers provided very useful feedback to this paper. JFL was supported by the SciDAC project from the Department of Energy. This research used resources of the National Energy Research Scientific Computing Center, which is supported by the Office of Science of the U.S. Department of Energy under contract DE-AC03–76SF00098. The National Center for Atmospheric Research is operated by the University Corporation for Atmospheric Research under sponsorship of the National Science Foundation.

References

Andrews, D. G., J. R. Holton, and C. B. Leovy (1987), *Middle Atmosphere Dynamics*, Academic, London.

Austin, J., and F. Li (2006), On the relationship between the strength of the Brewer-Dobson circulation and the age of stratospheric air, *Geophys. Res. Lett.*, *33*, L17807, doi:10.1029/2006GL026867.

Austin, J., and R. J. Wilson (2006), Ensemble simulations of the decline and recovery of stratospheric ozone, *J. Geophys. Res.*, *111*, D16314, doi:10.1029/2005JD006907.

Austin, J., J. Wilson, F. Li, and H. Vomel (2007), Evolution of water vapor concentrations and stratospheric age of air in coupled chemistry-climate model simulations, *J. Atmos. Sci.*, *64*, 905–921, doi:10.1175/JAS3866.1.

Baldwin, M. P., and M. Dameris (2007), Climate-ozone connections, in *Scientific Assessment of Ozone Depletion: 2006*, chap. 5, 572 pp., World Meteorol. Org., Geneva.

Brasseur, G. P., and S. Solomon (2005), *Aeronomy of the Middle Atmosphere*, 3rd ed., Springer, New York.

Butchart, N., et al. (2006), Simulations of the anthropogenic change in the strength of the Brewer-Dobson circulation, *Clim. Dyn.*, *27*, 727–741, doi:10.1007/s00382-006-0162-4.

Chipperfield, M. P., and W. Feng (2003), Comment on:Stratospheric ozone depletion at northern mid-latitudes in the 21st century: the importance of future concentrations of greenhouse gases nitrous oxide and methane, *Geophys. Res. Lett.*, *30*(7), 1389, doi:10.1029/2002GL016353.

Chipperfield, M. P., and F. E. Fioletov (2007), Global ozone: Past and future, in *Scientific Assessment of Ozone Depletion: 2006*, chap. 3, 572 pp., World Meteorol. Org., Geneva.

Chipperfield, M. P., and W. J. Randel (2003), Global ozone: Past and future, in *Scientific Assessment of Ozone Depletion: 2002*, chap. 4, 572 pp., World Meteorol. Org., Geneva.

Collins, W. D., et al. (2006), The Community Climate System Model version 3 (CCSM3), *J. Clim.*, *19*, 2122–2143, doi:10.1175/JCLI3761.1.

Considine, D. B., A. R. Douglass, P. S. Connell, D. E. Kinnison, and D. A. Rottman (2000), A polar stratospheric cloud parameterization for the Global Modeling Initiative three-dimensional model and its response to stratospheric aircraft, *J. Geophys. Res.*, *105*, 3955–3973, doi:10.1029/1999JD900932.

Dvortsov, V. L., and S. Solomon (2001), Response of the stratospheric temperatures and ozone to past and future increases in stratospheric humidity, *J. Geophys. Res.*, *106*, 7505–7514, doi:10.1029/2000JD900637.

Eyring, V., et al. (2006), Assessment of temperature, trace species, and ozone in chemistry-climate model simulations of the recent past, *J. Geophys. Res.*, *111*, D22308, doi:10.1029/2006JD007327.

Garcia, R. R., D. R. Marsh, D. E. Kinnison, B. A. Boville, and F. Sassi (2007), Simulation of secular trends in the middle atmosphere, 1950–2003, *J. Geophys. Res.*, *112*, D09301, doi:10.1029/2006JD007485.

Grooß, J.-U., and G. J. M. Russell III (2005), Technical note: A stratospheric climatology for O_3, H_2O, CH_4, NO_x, HCl, and HF derived from HALOE measurements, *Atmos. Chem. Phys.*, *5*, 2797–2807.

Hack, J. J., et al. (2006), Simulation of the global hydrological cycle in the CCSM Community Atmosphere Model Version 3 (CAM3): Mean features, *J. Clim.*, *19*, 2199–2221, doi:10.1175/JCLI3755.1.

Hall, T. M., and R. A. Plumb (1994), Age as a diagnostic of stratospheric transport, *J. Geophys. Res.*, *99*, 1059–1070, doi:10.1029/93JD03192.

Hall, T. M., D. W. Waugh, K. A. Boering, and A. R. Plumb (1999), Evaluation of transport in stratospheric models, *J. Geophys. Res.*, *104*, 18,815–18,839, doi:10.1029/1999JD900226.

Horowitz, L. W., et al. (2003), A global simulation of tropospheric ozone and related tracers: Description and evaluation of MOZART, version 2, *J. Geophys. Res.*, *108*(D24), 4784, doi:10.1029/2002JD002853.

Houweling, S., F. Dentener, and J. Lelieveld (1998), The impact of nonmethane hydrocarbon compounds on tropospheric photochemistry, *J. Geophys. Res.*, *103*, 10,673–10,696, doi:10.1029/97JD03582.

Kalnay, E., et al. (1996), The NCEP/NCAR 40-Year Reanalysis Project, *Bull. Am. Meteorol. Soc.*, *77*, 437–471, doi:10.1175/1520-0477(1996)077<0437:TNYRP>2.0.CO;2.

Kinnison, D. E., et al. (2007), Sensitivity of chemical tracers to meteorological parameters in the MOZART-3 Chemical Transport model, *J. Geophys. Res.*, *112*, D20302, doi:10.1029/2006JD007879.

Lack, D. A., X. X. Tie, N. D. Bofinger, A. N. Wiegand, and S. Madronich (2004), Seasonal variability of secondary organic aerosol: A global modeling study, *J. Geophys. Res.*, *109*, D03203, doi:10.1029/2003JD003418.

Lamarque, J.-F., J. T. Kiehl, P. G. Hess, W. D. Collins, L. K. Emmons, P. Ginoux, C. Luo, and X. X. Tie (2005), Response of a coupled chemistry-climate model to changes in aerosol emissions: Global impact on the hydrological cycle and the tropospheric burdens of OH, ozone and NO_x, *Geophys. Res. Lett.*, *32*(16), L16809, doi:10.1029/2005GL023419.

Minschwaner, K., et al. (1996), Bulk properties of isentropic mixing into the tropics in the lower stratosphere, *J. Geophys. Res.*, *101*, 9433–9439, doi:10.1029/96JD00335.

Newman, P. A., and M. Rex (2007), Polar ozone: Past and present, in *Scientific Assessment of Ozone Depletion: 2006*, chap. 4, 572 pp., World Meteorol. Org., Geneva.

Olsen, M. A., M. R. Schoeberl, and J. E. Nielsen (2007), Response of stratospheric circulation and stratosphere-troposphere exchange to changing sea surface temperatures, *J. Geophys. Res.*, *112*, D16104, doi:10.1029/2006JD008012.

Pétron, G., C. Granier, B. Khattatov, V. Yudin, J.-F. Lamarque, L. Emmons, J. Gille, and D. Edwards (2004), Monthly CO surface sources inventory based on the 2000–2001 MOPITT satellite data, *Geophys. Res. Lett.*, *31*, L21107, doi:10.1029/2004GL020560.

Randel, W. J., and F. Wu (2007), A stratospheric ozone profile data set for 1979–2005: Variability, trends, and comparisons with column ozone data, *J. Geophys. Res.*, *112*, D06313, doi:10.1029/2006JD007339.

Randel, W. J., F. Wu, S. J. Oltmans, K. Rosenlof, and G. E. Nedoluha (2004), Interannual changes of stratospheric water vapor and correlations with tropical tropopause temperatures, *J. Atmos. Sci.*, *61*, 2133–2148, doi:10.1175/1520-0469(2004)061<2133:ICOSWV>2.0.CO;2.

Randel, W. J., F. Wu, H. Vomel, G. E. Nedoluha, and P. Forster (2006), Decreases in stratospheric water vapor after 20001: Links to changes in the tropical tropopause and the Brewer-Dobson circulation, *J. Geophys. Res.*, *111*, D12312, doi:10.1029/2005JD006744.

Rasch, P. J., et al. (2006), Characteristics of atmospheric transport using three numerical formulations for atmospheric dynamics in a single GCM framework, *J. Clim.*, *19*, 2243–2266, doi:10.1175/JCLI3763.1.

Rayner, N. A., et al. (2003), Global analyses of sea surface temperature, sea-ice, and night marine air temperature since the late nineteenth century, *J. Geophys. Res.*, *108*(D14), 4407, doi:10.1029/2002JD002670.

Rind, D., J. Lerner, and C. McLindenn (2001), Changes of tracer distribution in the doubled CO_2 climate, *J. Geophys. Res.*, *106*, 28,061–28,079, doi:10.1029/2001JD000439.

Sander, S. P., et al. (2003), Chemical kinetics and photochemical data for use in atmospheric studies evaluation number 14, *Publ. 02–25*, Jet Propul. Lab., Pasadena, Calif.

Shindell, D. T., and V. Grewe (2002), Separating the influence of halogen and climate changes on ozone recovery in the upper stratosphere, *J. Geophys. Res.*, *107*(D12), 4144, doi:10.1029/2001JD000420.

Shindell, D. T., G. Faluvegi, N. Unger, E. Aguilar, G. A. Schmidt, D. M. Koch, S. E. Bauer, and R. L. Miller (2006), Simulations of preindustrial, present-day, and 2100 conditions in the NASA GISS composition and climate model G-PUCCINI, *Atmos. Chem. Phys.*, *6*, 4427–4459.

Uppala, S. M., et al. (2005), The ERA-40 re-analysis, *Q. J. R. Meteorol. Soc.*, *131*, 2961–3012, doi:10.1256/qj.04.176.

Waugh, D. W., and T. M. Hall (2002), Age of stratospheric air: theory, observations and models, *Rev. Geophys.*, *40*(4), 1010, doi:10.1029/2000RG000101.

Weatherhead, E. C., and S. B. Andersen (2006), The search for signs of recovery of the ozone layer, *Nature*, *441*, 39–45, doi:10.1038/nature04746.

West, J. J., A. M. Fiore, L. W. Horowitz, and D. L. Mauzerall (2006), Global health benefits of mitigating ozone pollution with methane emission controls, *Proc. Natl. Acad. Sci. U. S. A.*, *103*, 3988–3993, doi:10.1073/pnas.0600201103.

P. G. Hess, D. E. Kinnison, J.-F. Lamarque, and F. M. Vitt, Atmospheric Chemistry Division, Earth-Sun System Laboratory, National Center for Atmospheric Research, P.O. Box 3000, Boulder, CO 80307-3000, USA. (lamar@ucar.edu)